Journal of Medicinal Chemistry

Article

In silico driven design and synthesis of rhodanine derivatives as novel antibacterials targeting the enoyl reductase InhA

Liudas Slepikas, Gianpaolo Chiriano, Remo Perozzo, Sébastien Tardy, Agata Kranjc-Pietrucci, Ophélie Patthey-Vuadens, Hajer Ouertatani-Sakouhi, Sébastien Kicka, Christopher F. Harrison, Tiziana Scrignari, Karl Perron, Hubert Hilbi, Thierry Soldati, Pierre Cosson, Eduardas Tarasevicius, and Leonardo Scapozza

J. Med. Chem., **Just Accepted Manuscript** • DOI: 10.1021/acs.jmedchem.5b01620 • Publication Date (Web): 05 Jan 2016

In silico driven design and synthesis of rhodanine derivatives as novel antibacterials targeting the enoyl reductase InhA

Liudas Slepikas,[a,b†] Gianpaolo Chiriano,[a†] Remo Perozzo,[a] Sébastien Tardy,[a] Agata Kranjc-Pietrucci,[a] Ophélie Patthey-Vuadens,[a] Hajer Ouertatani-Sakouhi,[c] Sébastien Kicka,[d] Christopher F. Harrison,[e] Tiziana Scrignari,[f] Karl Perron,[f] Hubert Hilbi,[e,g] Thierry Soldati,[d] Pierre Cosson,[c] Eduardas Tarasevicius[b] and Leonardo Scapozza[a]*

[a]School of Pharmaceutical Sciences, Department of Pharmaceutical Biochemistry, University of Geneva and University of Lausanne, 30 Quai Ernest Ansermet, 1211 Geneva, Switzerland; [b] Faculty of Pharmacy, Lithuanian University of Health Sciences, LT 44307 Kaunas, Lithuania; [c]Department of cell physiology and metabolism, CMU, Rue Michel-Servet 1 1211 Geneva, Switzerland; [d]Department of Biochemistry, University of Geneva, 30 Quai Ernest Ansermet, 1211 Geneva, Switzerland; [e]Max von Pettenkofer Institute, Department of Medicine, Ludwig-Maximilians University Munich, 80336 Munich, Germany; [f]Microbiology Unit, Department of Botany and Plant Biology, University of Geneva, Switzerland; [g]Institute of Medical Microbiology, Department of Medicine, University of Zürich, Gloriastrasse 30/32, 8006 Zürich, Switzerland.

ABSTRACT

Here, we report on the design, synthesis and biological evaluation of 4-thiazolidinone (rhodanine) derivatives targeting *Mycobacterial tuberculosis* (*Mtb*) *trans*-2-enoyl-acyl carrier protein reductase (InhA). Compounds having bulky aromatic substituents at position 5 and a tryptophan residue at position *N*-3 of the rhodanine ring were the most active against InhA with IC_{50} values ranging from 2.7 μM to 30 μM. The experimental data showed consistent correlations with computational studies. Their antimicrobial activity was assessed against *Mycobacterium marinum* (*Mm*) (a model for *Mtb*), *Pseudomonas aeruginosa* (*Pa*), *Legionella pneumophila* (*Lp*) and *Enterococcus faecalis* (*Ef*), by using anti-infective, anti-virulence and antibiotic assays. 19 out of 34 compounds reduced *Mm* virulence at 10 μM. **33** exhibited promising antibiotic activity against *Mm* with a MIC of 0.21 μM and showed up to 89% reduction of *Lp* growth in an anti-infective assay at 30 μM. **32** showed high antibiotic activity against *Ef* with a MIC of 0.57 μM.

INTRODUCTION

Infectious diseases are a serious threat worldwide as emerging bacterial resistances to antibiotics raises concerns about the use of antibacterial agents in clinical practice.[1] Thus, the search for new drugs effective for the treatment of bacterial infections is of high priority. Focusing on known validated intracellular targets remains a valid approach to identify new drug candidates with novel chemical structures.[2] One of the strategies adopted to control bacterial pathogens is to target the biosynthesis pathway of fatty acids (FAS-II), in which the highly conserved enoyl-acyl carrier protein reductase (InhA) plays a key role.[3] The suitability of targeting InhA for combating tuberculosis has been validated by the first-line antitubercular drug isoniazid, a very powerful mycobacterial InhA inhibitor.[4] Furthermore, the catalytic domain of InhA is well characterized and amenable for structure-based drug design. Since isoniziad, a pro-drug converted by catalase-peroxidase (KatG) into an InhA inhibitor, was introduced in 1952, the rising resistance in clinical practice due to KatG modifications calls for the discovery of new drugs acting directly against InhA.[5] Indeed, isoniazid-related *Mycobacterium* resistance has been reported to be mainly associated with the KatG and not with the InhA protein.[6] These findings indicate that targeting mycobacterial InhA and its orthologs in other pathogens remains a suitable strategy for developing compounds against tuberculosis and other bacterial infections. Based on several ligand- or structure-based approaches, different classes of InhA inhibitors have been developed, such as diphenyl ethers related to triclosan,[7] pyrrolidine carboxamides,[8] INH-NAD analogs[9] and pyridomycin.[10] However, only a few of them inhibited *Mtb* growth *in vitro*.[11]

In this article, we describe the *in silico* analysis-based rational design, synthesis and characterization of InhA inhibitors bearing rhodanine as a privileged scaffold. The inhibitory effect of the rationally designed rhodanine derivatives against *Mm* was analyzed using both anti-virulent and antibiotic assays. Interestingly, these compounds also inhibited the growth of other Gram-positive (*Ef*) and Gram-negative (*Lp*) pathogenic bacteria.

RESULTS AND DISCUSSION

Design and Chemical Space Exploration

As a first step towards the discovery of novel InhA inhibitors, we identified a moiety chemically accessible for designing and synthesizing a consistent library of compounds to be biologically evaluated. We focused on the rhodanine moiety for the following reasons: i) rhodanine represents a privileged structure as several derivatives have been reported to be pharmacologically active against various bacterial targets, such as UDP-galactopyranose mutase,[12] UDP-*N*-acetylmuramoyl-L-alanine synthetase,[13] nucleoside diphospho-glycosyltransferase,[14] penicillin-binding proteins,[15] C class β-lactamase,[16] RNA polymerase,[17] dihydrolipoamide acyltransferase,[18] anthrax lethal factor,[19] botulinum neurotoxins[20] and the bacterial oxyreductase class of enzymes;[21] ii) the rhodanine scaffold is amenable to parallel synthesis of differently polysubstituted derivatives. While many rhodanine derivatives have been designed previously, none of them has been reported to target bacterial InhA. However, inhibition of the homologous *Plasmodium falciparum* FabI has been studied using compounds bearing the rhodanine scaffold.[22]

Based on these considerations, we designed, synthesized and screened a first series of compounds (**1-20**) (see Chart 1). The initial screening of derivatives **1-20** was performed at 30 μM to reveal compounds with a promising inhibitory profile against InhA (the data of the most active derivatives are shown in Figure 1, and the complete data set can be found in Table S1 of the supporting material). The results clearly show that several of the designed compounds strongly inhibit InhA (Figure 1). The results suggest some trends in term of structure-activity relationship. In this respect, the first observation is that increased lipophilicity probably plays an important role in modulating InhA inhibitory activity, as all tested derivatives bearing bulky lipophilic substituents at position 5 (derivatives **13-18**) and *N*-3 of the rhodanine ring (derivatives **12-14**, **16-17)** show higher or even complete inhibition of the enzyme at 30 μM (Figure 1). In particular, the presence of a tryptophan residue at position *N*-3 of the rhodanine

ring, e.g. in derivatives **12** and **17,** seems to be very favorable for the InhA inhibitory activity (Figure 1).

Rationale of Structure-Based Design

Compounds with the highest inhibitory activity were investigated by molecular docking simulations, carried out with GOLD software (5.2.2 version),[23] to identify their putative binding modes within the active site of InhA and help to further design the series of compounds. The binding mode of derivative **12** at the InhA binding pocket is representative of the first series of compounds and is reported in Figure 2. The oxygen of the carbonyl group (C-4) within the rhodanine ring interacts via H-bond with the phenolic hydroxyl group of Tyr158 and the 2′-hydroxyl group of the nicotinamide ribose (Figure 2). Furthermore, the docking reveals that the arylidene substituent at position 5 of the rhodanine ring is directed towards the end of the InhA binding pocket and interacts hydrophobically with the side chains of Met199, Ile215, and Leu218 (Figure 2). Remarkably, the enhanced bulkiness and hydrophobicity of the substituent of **17** at position 5 (4-dimethylamino-naphtylidene) compared to **12** (4-dimethylamino-benzylidene) induces a better occupancy of the pocket. This correlates well with increased inhibitory activity of **17** when compared with that of **12**. The tryptophan residue of compound **12** is directed towards the solvent-exposed entry site of InhA with its carboxyl moiety pointing towards the NAD+ phosphate bridge. Depending on the protonation state of the ligand or the NAD+ within the binding site, the observed position of the carboxyl moiety could eventually lead to the formation of an additional hydrogen bond.

Based on the above-mentioned findings, we designed and synthesized a second series of rhodanine derivatives (**21-30**, **32-34**) starting from compounds **12** and **17** to explore the lipophilic interactions within the accessible hydrophobic cavity.

Chemistry

The synthesis of the designed compounds, **1-34** (Chart 1), was performed as presented in Scheme 1. Selected amino acids with different polarity and size were used as starting materials for synthetizing derivatives **1-5**, **19-20** and **6-18**, **21-34.** The reaction of the carbon disulfide with the amino acids in the presence of potassium hydroxide in aqueous solution yielded amino acid dithiocarbamates. Further reaction of the latest with potassium chloroacetate and cyclization with hydrochloric acid led to rhodanine ring formation with the amino acid moiety attached to the nitrogen at position 3 (*N*-3) . All intermediate rhodanine derivatives bearing amino acids at the position *N*-3 were synthesized as described in the literature[24] and used directly, without prior purification, for the synthesis of the final compounds **1-34** by Knoevenagel condensation between *N*-substituted rhodanine derivatives and different aldehydes in acetic acid in the presence of a catalytic amount of sodium acetate. The identity of the final compounds was verified by FTIR, ^{1}H-NMR, ^{13}C-NMR and HRMS.

Improved InhA Inhibition for the Designed Second Series of Rhodanine Derivatives

Based on the initial screening data of the first series of rhodanine-containing compounds, **1-20**, and driven by molecular docking studies we then designed and synthesized a second series of derivatives, **21-34** (Chart 1). Subsequent evaluation of their inhibitory activity at a fixed concentration of 30 μM showed an improved *Mtb* InhA inhibitory profile (Figure 1).

The screening results revealed that compounds carrying bulky substituents at position 5 of the rhodanine ring **32-34** were more active, in agreement with what has been predicted by modeling. In general, 10 out of the 14 newly synthesized compounds (**21-34**), showed complete InhA inhibition at 30 μM. Notably, a strong correlation between *in silico* prediction and *in vitro* analysis was observed for the derivatives bearing a tryptophan moiety at position *N*-3 of the rhodanine scaffold, i.e. compounds **24-30** and **32-34**; This finding is in line with the observation that tryptophan plays an important role for the activity against InhA compared to the synthetic derivatives **1-11**, **13-16**, **18** and **20-23,** which all

harbor other amino acids at position *N*-3. The IC_{50} values for the most active InhA inhibitors (**12**, **16**, **21-22**, **25-30**, **32-34**) were determined and found to be in the range of ~3-28 μM (see Table 1). The most potent inhibitor, compound **32,** showed an IC_{50} of 2.9 ± 0.7 μM which is about twice as potent as the reference compound triclosan (IC_{50} of 6.1 ± 2.1 μM).

Structure-Activity Relationship (SAR) Studies

Molecular modeling studies allowed us to improve and potentially correlate the results from the inhibition studies with the docking-based binding poses. In particular, the computational analysis of compound **33** revealed that the introduction of more bulky 4-methyl-naphthylidene substituent at the position 5 of the rhodanine ring does not affect the key H-bond interactions between the carbonyl group of the rhodanine with the hydroxyl group of Tyr158 and with the 2′-hydroxyl group of the nicotinamide ribose (Figure 2, Figure 3). Furthermore, the carboxyl group of tryptophan is positioned in a favorable manner to eventually form additional hydrogen bonds with NAD^+ phosphate (Figure 3). As with the first series of derivatives, **1-20**, arylidene or more bulky naphthylidene substituents occupy the fatty acid binding pocket of the InhA binding site. Moreover, derivatives bearing bulky lipophilic substituents form hydrophobic interactions with the side chains of Phe149, Met199, Ile215, Leu218, and Met155 located in the InhA binding pocket (Figures 2 and 3).

The SAR of the synthesized compounds revealed the importance of substituents at positions 5 and *N*-3 of rhodanine in InhA inhibition. Derivatives **12**, **17** and **24-30**, **32-34** with tryptophan linked to *N*-3 were very active, and hence the indolyl moiety appeared to be the most effective substituent (Figure 1). In contrast, derivatives **1-3** and **20** bearing small (short chain) amino acids, e.g. α-alanine, β-alanine, or α-aminobutyric acid, or a second carboxyl group (compound **11**) did not show any significant inhibition (Chart 1, Figure 1). Similarly, derivatives **4-5** and **6-8** harboring small lipophilic side chains (e.g., leucine, nor-leucine) displayed low inhibitory activity. In general, derivatives consisting of amino acids with branched (valine, leucine, isoleucine, **3-6**) or non-branched side chains (nor-valine, nor-leucine, **7-**

8) did not exhibit significantly different inhibitory activity towards InhA. However, the side chain length of amino acid residues appeared to be important in modulating the activity of derivatives **13-16** harboring the 1-dimethyl-naphthylidene group as substituent in position 5 of rhodanine (Figure 1). In particular compound **16** carrying a nor-leucine moiety was very potent against InhA while the analog **15** bearing a nor-valine side chain was inactive. Furthermore, replacing the sulfur atom in methionine with the more bulky selenium (derivatives **9** and **10**) did not lead to any significant change in activity.

In agreement with the single dose inhibition data (Figure 1) the InhA inhibition dose-response experiments (see Table 1) data show that the presence of the tryptophan substituent at *N*-3 of rhodanine (derivatives **12**, **17**, **24-30**, **32-34**) correlates with an increase of the InhA inhibitory activity of the compounds. Thus, the most potent inhibitors presented in this work share the tryptophan moiety at *N*-3.

Further investigations with respect to the impact of aromatic substituents at the position 5 of rhodanine showed that the presence of an extended bulky aliphatic chain in para position of the benzylidene group (compounds **21**, **24-28**) is important for the InhA activity of the compounds while a smaller substitution leads to a decreased activity (compounds **22-23**).

In agreement with the *in silico* postulated binding mode, the *in vitro* data indicate that the improved inhibitory activity of the synthesized derivatives is strongly related to the possibility of increasing hydrophobic interactions in the binding pocket of InhA (Figure 2B, Figure 3). This was clearly confirmed by comparing compounds carrying the dimethylamino group (derivatives **4**, **21**) with those having the more lipophilic diethylamino moiety (derivatives **12**, **24**) in para position of the benzylidene. The more lipophilic substituent in the para position shows a higher inhibitory activity at 30 μM (Figure 1). However, replacing the diethylamino group with more lipophilic longer aliphatic substituents (compounds **25-26**) did not significantly improve the inhibitory activity suggesting that the increase of flexibility due to longer aliphatic chain is reducing the impact of the enhanced hydrophobic interactions. In line with the postulated binding mode, the compound with a bulky and hydrophobic chlorine in para position (derivative **29**) showed similar activity compared to the one having the diethylamino group (IC_{50}

of 19.7 ± 1.4 μM). This activity could be improved about twofold to reach an IC_{50} value of 9.5 ± 2.2 μM with the introduction of a second chlorine atom in ortho (derivative **30**). The trend observed with compound **30** and the modelling showing that a proximal rigid bulky group at position 5 of the rhodanine is favorable for the inhibition activity led us to synthetize derivatives **32-24** where the benzylidene moiety is replaced by the bulkier and hydrophobic anthracenylidene or naphthylidene group. The inhibitory activity data confirmed the hypothesis as compound **32** is the strongest InhA of the series with an IC_{50} value of 2.9 ± 0.7μM. In line with the established SAR the introduction of a small fluorine atom in the para position (**23**) caused a loss of activity (Figure 1).

Overall, on the basis of inhibition data at 30 μM (Figure 1) confirmed by the IC_{50} value of the dose-response experiments (Table 1), among the synthesized compounds those with the polycyclic aromatic substituents at position 5 of the rhodanine ring were the most active ones (see **13-14**, **16-18**, **32-34**). These results strongly correlate with the *in silico* data showing bicyclic (derivatives **13-18**, **33-34**) and tricyclic substituents (derivative **32**) to interact strongly via their large surface area with the hydrophobic pocket of the InhA binding site (Figure 2 and Figure 3). Interestingly, the absence of the carboxyl group in the tryptophan moiety (compound **31**) led to loss of activity.

Antibiotic and Anti-Infective Effects on Pathogenic Bacteria

The antimicrobial potential of the compound series was further tested towards the pathogenic bacteria *Mm*, *Pa*, *Lp* and *Ef*, using cell-based antibiotic and anti-infection assays. To this end we further investigated the most powerful InhA inhibitors, compounds **12**, **16-18**, **21**, **24-30**, and **32-34,** by determining their antibiotic effect expressed measuring MIC against *Mm* at concentrations ranging from submicromolar to submillimolar. These experiments show that most of the derivatives possessed anti-*Mm* activity with MIC ranging from 0.2 to 185 μM (Table 1). Compound **24** bearing a longer aliphatic chain (diethylamino) at the para position was more active than **12** with the shorter dimethylamino group. Replacement of the diethylamino group with the aliphatic propyl chain (derivatives **25** and **27**)

did not increase anti-*Mm* activity. Moreover, introduction of chlorinated substituents (derivatives **29** and **30**) did not increase activity. Yet, lipophilic substituents at position 5 of the rhodanine seemed to play an important role, as the derivatives **15** and **33-34**, bearing the naphthylidene fragment, were most active against *Mm*. Notably, the chirality of the tryptophan residue introduced on the *N*-3 position of the rhodanine moiety was particularly relevant when comparing compounds **25**, **26** and **33** (L-tryptophan) with their corresponding R enantiomers used to synthesize **27**, **28** and **34** (D-tryptophan). Indeed, compounds **26** and **33** showed a 10-fold higher anti-*Mm* activity than **28** and **34** (Table1). If we compare compounds having similar logP, we clearly see that an increased inhibitory activity on the isolated enzyme results in lower MIC values against *Mm*. This supports the idea that InhA is a relevant target for the antibiotic activity of the rhodanine derivatives.

Derivative **32** bearing a tricyclic 10-chloro-anthracenylidene ring did not show a significant effect against *Mm* most likely due to very high logP (calculated LogP = 5.98; http://www.molinspiration.com) causing the trapping of the molecule into the membrane lipid of *Mm*.

In addition, the compounds were tested against *Mm* in a recently developed assay using *Dictyostelium discoideum* amoebae growth as an inverse measure of the pathogen virulence.[25] *Dictyostelium* cannot grow on a mixed bacterial lawn of *Mm* and *Klebsiella pneumoniae* (*Kp*). However, 19 out of 34 rhodanine derivatives (~56%) were able to reduce *Mm* virulence at a concentration of 10 µM. The results are shown in Table 1 whereas the complete data set is presented in supplementary Table S2. Indeed, upon treatment with, compounds such as **17**, **18**, **21**, **24-30** and **32-34** (Table 1), *Dictyostelium* grew by feeding on *Kp* and formed phagocytic plaques in presence of M*m*. Those compounds were not toxic to the host and allowed *Dictyostelium* to proliferate. Therefore, these rhodanine compounds specifically attenuated the virulence of *Mm* without affecting *Kp* that feeds *Dictyostelium*.

Recently, gemfibrozil was reported to inhibit the intracellular growth of *Lp* in macrophages by targeting in a noncompetitive manner FabI, the *Lp* orthologue of *Mtb* InhA.[26] These findings prompted us to test the rhodanine derivatives against *Lp* (Figure 4).[27] 29 compounds (~85%) possessed the capacity to de-

crease axenic *Lp* growth at 30 μM. Interestingly, the same SAR pattern as found for *Mm* was observed for *Lp*, strongly suggesting *Lp*FabI to be the target of these rhodanine derivatives. Accordingly, the impact of different amino acids at position *N*-3 could clearly be identified. Synthetic compounds having a β-amino acid (**20**), methionine (**10**), phospholeucine (**18**) or derivatives without a carboxylic group (**19** and **31**) were less active than the others. Also in the case of *Lp*FabI, the indolyl moiety appeared to be the most effective substituent. With the exception of compound **28**, all the ligands bearing this group strongly inhibited axenic *Lp* growth. Furthermore, by increasing the bulkiness of substituents at position 5 of rhodanine, as in derivatives **13-18** and **32-34**, the inhibitory activity against *Lp* was retained.

The compounds series was also tested against the intracellular growth of *Lp* using the established *Acanthamoeba castellanii* - *Lp* host-pathogen system.[27] Using this system, the compounds **25**, **27**, and **33-34**, all of them bearing the tryptophan residue, showed remarkable activity against intracellular replication of *Lp*. In particular, the most active compound, derivative **33**, reduced the growth of *Lp* by 89%. Moreover, compounds **33-34** bearing naphthylidene, were more active if compared to the ones with the arylidene substituent, and the bulky naphthylidene substituent (**33**) was the most effective against *Lp* growing in the host cell. On the other hand, inactivity of all other synthetic compounds in this infection assay might be due to poor penetration through the amoeba cell membrane, possible inactivation inside or activity of pumps transporting the drugs out of the cell.

Antibacterial activity against *Ef* and *Pa* was also investigated via the serial broth dilution antibiotic assay (Table 1). The synthetic rhodanine derivatives **1-34** were all inactive against the Gram-negative pathogen *Pa*. In contrast, the compounds **32-34** were effective against *Ef* with MIC values ranging from 0.57 μM to 5.2 μM. The growth inhibition of the derivative with the lowest IC_{50} value against InhA, a homolog of *Ef* FabI (62% homology), compound **32** (harboring the tricyclic 10-chloroanthracenylidene fragment), was also the most active molecule against *Ef* in the *in vitro* assay (Table 1).

CONCLUSIONS

Thirty-four rhodanine derivatives, characterized by carrying amino acid residues at the position *N*-3, were synthesized and their inhibitory activity was evaluated against *Mtb* InhA. Enzymatic data together with molecular modeling results supported InhA to be a possible target of the rhodanine derivatives. The potential putative binding modes/affinities between selected ligands and the target enzyme InhA were identified. The most promising compounds showed both antibiotic and anti-virulent activity against *Mm* and, in particular, the compounds **32-34**, also exhibited remarkable activity against *Ef*. Several compounds showed a strong antibiotic effect, and some of them reduced the intracellular replication of *Lp*. Furthermore, derivative **33,** the most potent compound, showed broad range activity in all *in vitro* experiments and might represent a good starting point for optimizing the structure to develop more active antibacterials.

In conclusion, the results obtained in this work highlight amino acid substituted rhodanines as very promising antibacterial scaffolds acting through enoyl-acyl carrier protein reductases inhibition. This study suggests that the development of more potent enoyl-acyl carrier protein reductases inhibitors could lead to novel broad-spectrum antibacterial drug candidates.

EXPERIMENTAL PROCEDURES

Reagents and Analytical Procedures

Solvents and reagents were used without further purification. The progress of all reactions was monitored by TLC on precoated silica gel plates (Merck Silica gel 60 F254). The developed chromatograms were viewed under UV light at 254 nm. For preparative thin layer chromatography 20×20 cm TLC plates (1 mm) from Analtech were used. All ^{1}H NMR and ^{13}C NMR spectra were acquired on a Varian 300 operating at 300 and 75 MHz, respectively. The proton spectra were referenced to the respective residual solvent peaks (DMSO-d_6, 2.50 ppm) except for those recorded in $CDCl_3$ (7.26 ppm). Carbon spectra were referenced to the central peak of the respective residual solvents (DMSO-d_6 39.50; $CDCl_3$ 77.0 ppm). High-resolution mass spectra were obtained using electrospray ionization (ESI) and QSTAR Pulsar (AB/MDS Sciex) mass spectrometer. Infrared (IR) spectra were measured on a Perkin Elmer FTIR 100 spectrophotometer using ATR. Melting points were determined in a Büchi B-540 melting point apparatus and are uncorrected. To assess the purity of the reported compounds, 1 mg of each one of them was weighed and dissolved in 50 ml of acetonitrile. The sample was filtered and analysed by HPLC analysis using the Agilent 1200 series with Agilent Zorbax RRHD column C18 column (1.8 µm, 2.1 mm x 50 mm) and applying a flow rate of 0.4 mL/min and an injection volume of 1 µL. The mobile phase was composed of solution A (0.1% formic acid in water) and solution B (acetonitrile), and different gradient conditions were applied (details are shown in the SI material). DAD-UV detection was performed at the wavelength of 410 nm or 474 nm. The purity of the active compounds is ≥95%, being the Z isomer the most prevalent one accordingly to the ^{1}H-NMR analysis.

General Procedure for Preparation of (4-oxo-2-thioxothiazolidin-3-yl)-Amino Acids Derivatives.

2-(4-oxo-2-thioxothiazolidin-3-yl)-amino acid derivatives were synthesized according to the general procedures described in the literature.[24] In a round-bottom flask equipped with a magnetic stirrer, amino acid (30 mmol) was dissolved with potassium hydroxide (30 mmol) in water (30 mL). Carbon di-

sulfide CS_2 (30 mmol) was added to the reaction mixture, which was stirred for 2-6 hours. An aqueous solution of potassium chloroacetate (30 mmol) was added and stirring was continued at room temperature for 30 minutes. Then the reaction mixture was acidified with 2N HCl until pH 2.0-3.0 and heated to 90 °C for 5-30 minutes. The reaction mixture was poured in cold water and precipitated intermediate was used for the synthesis of targeted compounds without any further purification.

General Procedure for Preparation of 5-yliden (4-oxo-2-thioxothiazolidin-3-yl)-Amino Acids Derivatives by Knoevenagel Condensation. 10 mmol of 2-(4-oxo-2-thioxothiazolidin-3-yl)-amino acid derivative were solubilized with 10 mL acetic acid and 300 mg of AcONa and 11 mmol of appropriate aldehyde were added and heated overnight. The reaction mixture was poured in cold water, precipitated solid was filtered, washed with a small amount of AcOH, EtOH, Et_2O and dried. The derivatives were purified by crystallization from acetic acid or by preparative thin layer chromatography.

(2*S*)-{(5*Z*)-5-[4-(Dimethylamino)benzylidene]-4-oxo-2-thioxo-1,3-thiazolidin-3-yl}propanoic acid (1).[27] Red solid, 48% yield. M.p. 248-252 °C, from acetic acid. ^{1}H-NMR (DMSO-d_6) δ 7.63 (s, 1H), 7.43 (d, J = 9.0 Hz, 2H), 6.80 (d, J = 9.0 Hz, 2H), 5.55 (q, J = 7.1 Hz, 1H), 3.01 (s, 6H), 1.50 (d, J = 7.1 Hz, 3H). ^{13}C-NMR (DMSO-d_6) δ 170.4, 166.93, 166.93, 152.70, 135.73, 133.97, 120.43, 113.53, 113.22, 52.99, 40.20, 14.22. FTIR - 2880, 1693, 1611, 1568, 1522, 1437, 1376, 1340, 1305, 1249, 1229, 1213, 1186, 1115, 1076, 997, 923, 808, 741, 681 cm^{-1}. HRMS (ESI$^+$): calcd. 337.0675 for $C_{15}H_{17}N_2O_3S_2$ $[M+H]^+$; Found: 337.0676.

(2*S*)-{(5*Z*)-5-[4-(Dimethylamino)benzylidene]-4-oxo-2-thioxo-1,3-thiazolidin-3-yl}butanoic acid (2). Red solid, 40% yield. M.p. 189-191 °C, from acetic acid. ^{1}H-NMR (DMSO- d_6) δ 7.64 (s, 1H), 7.44 (d, J = 8.6 Hz, 2H), 6.78 (d, J = 8.6 Hz, 2H), 5.43 (t, J = 7.3 Hz, 1H), 3.01 (s, 6H), 2.27-2.07 (m, 2H), 0.78 (t, J = 7.3 Hz, 3H). ^{13}C-NMR (DMSO- d_6) δ 193.73, 169.97, 167.26, 152.70, 135.79, 133.54,

120.45, 113.28, 112.91, 59.42, 40.42, 21.73, 11.34. FTIR - 2976, 2890, 2698, 1610, 1574, 1525, 1436, 1374, 1328, 1274, 1231, 1205, 1180, 1127, 1063, 952, 908, 806, 788, 740 cm^{-1}. HRMS (ESI^+): calcd 351.0831 for $C_{16}H_{19}N_2O_3S_2$ $[M+H]^+$; Found: 351.0837.

(2*R*,*S*)-{(5*Z*)-5-[4-(Dimethylamino)benzylidene]-4-oxo-2-thioxo-1,3-thiazolidin-3-yl}-3-methylbutanoic acid (3). Red solid, 60% yield. M.p. 210-212 °C, from acetic acid. ^{1}H-NMR (DMSO-d_6) δ 7.7 (s; 1H), 7.47 (d, *J* = 8.7 Hz, 2H), 6.83 (d, *J* = 8.7 Hz, 2H), 5.16 (d, *J* = 8.5 Hz, 1H), 3.04 (s, 6H), 2.84-2.63(m, 1H), 1.19 (d, *J* = 6.3 Hz, 3H), 0.72 (d, *J* = 6.7 Hz, 3H). ^{13}C-NMR (DMSO-d_6) δ 193.45, 169.54, 167.33, 152.80, 136.28, 134.13, 120.37, 112.92, 112.79, 62.54, 27.75, 22.45, 19.54. FTIR - 2967, 2888, 1726, 1686, 1616, 1573, 1528, 1470, 1441, 1377, 1326, 1286, 1254, 1230, 1211, 1186, 1127, 897, 800, 744, 688 cm^{-1}. HRMS (ESI^+): calcd 365.0988 for $C_{17}H_{21}N_2O_3S_2$ $[M+H]^+$; Found: 365.0988.

(2*R*)-2-{(5*Z*)-5-[4-(Dimethylamino)benzylidene]-4-oxo-2-thioxo-1,3-thiazolidin-3-yl}-4-methylpentanoic acid (4). Red solid, 52% yield. M.p. 100-102 °C, from acetic acid. ^{1}H-NMR (DMSO-d_6) δ 7.68 (s, 1H), 7.47 (d, *J* = 9 Hz, 2H), 6.83 (d, *J* = 9 Hz, 2H), 5.56 (m, 1H), 3.05 (s, 6H), 2.22-1.99 (m, 2H), 1.51-1.33 (m, 1H), 0.92 (d, *J* = 6,6 Hz, 3H), 0.85 (d, *J* = 6.6 Hz; 3H). ^{13}C-NMR (DMSO-d_6) δ 193.56, 170.25, 167.32, 152.77, 136.01, 134.07, 120.41, 111.75, 111.70, 56.54, 37.17, 25.46, 23.61, 22.67. FTIR - 2954, 1696, 1611, 1563, 1519, 1437, 1338, 1273, 1213, 1183, 1131, 1096, 944, 809, 744 cm^{-1}. HRMS (ESI^+): calcd 379.1144 for $C_{18}H_{23}N_2O_3S_2$ $[M+H]^+$; Found: 379.1143.

(2*S*)-2-{(5*Z*)-5-[4-(Dimethylamino)benzylidene]-4-oxo-2-thioxo-1,3-thiazolidin-3-yl}-4-methylpentanoic acid (5). Red solid, 49% yield. M.p. 180-182 °C, from acetic acid. ^{1}H-NMR (DMSO-d_6) δ 7.68 (s, 1H), 7.48 (d, *J* = 9.0 Hz, 2H), 6.84 (d, *J* = 9.0 Hz, 2H), 5.58-5.47 (m, 1H), 3.04 (s, 6H), 2.22-1.99 (m, 2H), 1.51-1.33 (m, 1H), 0.92 (d, *J* = 6.6 Hz, 3H), 0.85 (d, *J* = 6.6 Hz, 3H). ^{13}C-

NMR (DMSO-d_6) δ 193.50, 170.26, 167.30, 152.79, 136.10, 134.10, 120.39, 113.0, 112.95, 56.36, 37.17, 25.53, 23.60, 22.67. FTIR - 2955, 1695, 1611, 1561, 1519, 1437, 1338, 1272, 1212, 1169, 1126, 1095, 944, 807, 742, 680 cm^{-1}. HRMS (ESI^+): calcd 379.1144 for $C_{18}H_{23}N_2O_3S_2$ $[M+H]^+$; Found: 379.1153.

(2*S*)-2-{(5*Z*)-5-[4-(Dimethylamino)benzylidene]-4-oxo-2-thioxo-1,3-thiazolidin-3-yl}-3-methylpentanoic acid (6). Red solid, 55% yield. M.p. 193-195 °C, from acetic acid. ^{1}H-NMR ($CDCl_3$) δ 7.65 (s, 1H), 7.39 (d, *J* = 9.0 Hz, 2H), 6.72 (d, *J* = 9.0 Hz, 2H), 5.46 (d, *J* = 9.5 Hz, 1H), 3.08 (s, 6H), 2.75-2.56 (m, 1H), 1.34-0.94 (m, 2H), 1.26 (d, *J* = 6.6 Hz, 3H), 0.85 (t, *J* = 7.2 Hz, 3H). ^{13}C-NMR ($CDCl_3$) δ 193.37, 172.45, 168.13, 152.29, 135.83, 133.39, 120.97, 112.22, 114.32, 62.07, 40.29, 22.83, 25.33, 17.71, 11.31. FTIR - 2954, 1693, 1611, 1562, 1519, 1436, 1332, 1271, 1211, 1167, 1094, 943, 809 cm^{-1}. HRMS (ESI^+): calcd 379.1144 for $C_{18}H_{23}N_2O_3S_2$ $[M+H]^+$; Found: 379.1142.

(2*R*,*S*)-2-{(5*Z*)-5-[4-(Dimethylamino)benzylidene]-4-oxo-2-thioxo-1,3-thiazolidin-3-yl}pentanoic acid (7). Red solid, 53% yield. M.p. 250-251 °C, from acetic acid. ^{1}H-NMR (DMSO-d_6) δ 7.65 (s, 1H), 7.44 (d, *J* = 9.0 Hz, 2H), 6.79 (d, *J* = 9 Hz, 2H), 5.59-5.45 (m, 1H), 3.02 (s, 6H), 2.27-1.99 (m, 2H), 1.32-1.06 (m, 2H), 0.84 (t, *J* = 7.3 Hz, 3H). ^{13}C-NMR (DMSO-d_6) δ 193.49, 169.94, 167.21, 152.74, 136.01, 134.05, 120.41, 113.11, 113.01, 57.68, 28.50, 27.95, 22.52, 14.44. FTIR - 2882, 1689, 1616, 1572, 1525, 1437, 1374, 1329, 1266, 1209, 1184, 1124, 1059, 944, 801, 745 cm^{-1}. HRMS (ESI^+): calcd 365.0988 for $C_{17}H_{21}N_2O_3S_2$ $[M+H]^+$; Found: 365.0979.

(2*R*,*S*)-2-{(5*Z*)-5-[4-(Dimethylamino)benzylidene]-4-oxo-2-thioxo-1,3-thiazolidin-3-yl}hexanoic acid (8). Red solid, 61% yield. M.p. 196-198 °C, from acetic acid. ^{1}H-NMR (DMSO-d_6) δ 7.65 (s, 1H), 7.44 (d, *J* = 9.0 Hz, 2H), 6.80 (d, *J* = 9.0 Hz, 2H), 5.60-5.42 (m, 1H), 3.02 (s, 6H), 2.26-2.04 (m, 2H), 1.34-1.00 (m, 4H), 0.79 (t, *J* = 7.0 Hz, 3H). ^{13}C-NMR (DMSO-d_6) δ 193.49, 169.94, 167.21, 152.74,

136.01, 134.05, 120.41, 113.11, 113.01, 57.68, 28.50, 27.96, 22.52, 14.44, 14.41. FTIR - 2915, 1856, 1693, 1612, 1563, 1520, 1441, 1372, 1337, 1298, 1253, 1222, 1185, 1118, 1095, 942, 905, 820, 806, 681 cm^{-1}. HRMS (ESI^+): calcd 379.1144 for $C_{18}H_{23}N_2O_3S_2$ $[M+H]^+$; Found: 379.1136.

(2*R*,*S*)-2-{(5*Z*)-5-[4-(Dimethylamino)benzylidene]-4-oxo-2-thioxo-1,3-thiazolidin-3-yl}-4-(methylsulfanyl)butanoic acid (9). Red solid, 56% yield. M.p. 152-154 °C, from acetic acid. ^{1}H-NMR (DMSO-d_6) δ 7.65 (s, 1H), 7.45 (d, J = 9.0 Hz, 2H), 6.80 (d, J = 8.8 Hz, 2H), 5.79-5.61 (m, 1H), 3.02 (s, 6H), 2.51-2.30 (m, 4H), 1.99 (s, 3H). ^{13}C-NMR (DMSO-d_6) δ 193.55, 169.85, 167.36, 152.74, 135.84, 134.02, 120.44, 113.46, 112.44, 56.72, 40.28, 30.83, 27.84, 15.27. FTIR - 2910, 1722, 1691, 1611, 1567, 1521, 1436, 1316, 1252, 1252, 1228, 1189, 1102, 942, 803, 685 cm^{-1}. HRMS (ESI^+): calcd 397.0708 for $C_{17}H_{21}N_2O_3S_3$ $[M+H]^+$; Found: 397.0704.

(2*S*)-2-{(5*Z*)-5-[4-(Dimethylamino)benzylidene]-4-oxo-2-thioxo-1,3-thiazolidin-3-yl}-4-(methylselenyl)butanoic acid (10). Red solid, 40% yield. M.p. 88-90 °C, from acetic acid. ^{1}H-NMR (DMSO-d_6) δ 7.62 (s, 1H), 7.44 (d, J = 8.7 Hz, 2H), 6.81 (d, J = 8.7 Hz, 2H), 5.70-5.48 (m, 1H), 3.02 (s, 6H), 2.57-2.35 (m, 3H, overlaping with DMSO) 1.96-1.82 (m, 4H). ^{13}C-NMR (DMSO-d_6) δ 193.79, 169.87, 167.41, 152.77, 135.49, 134.03, 120.52, 113.92, 112.93, 58.42, 40.28, 29.09, 22.08, 4.31. FTIR - 2919, 1694, 1611, 1562, 1519, 1437, 1338, 1293, 1338, 1293, 1226, 1170, 1148, 1098, 943, 810 cm^{-1}. HRMS (ESI^+): calcd 445.0153 for $C_{17}H_{21}N2O_3S_2Se$ $[M+H]^+$; Found: 445.0163.

(2*S*)-2-{(5*Z*)-5-[4-(Dimethylamino)benzylidene]-4-oxo-2-thioxo-1,3-thiazolidin-3-yl}butanedioic acid (11). Red solid, 45% yield. M.p. 274-275 °C, from acetic acid. ^{1}H-NMR (DMSO-d_6) δ 7.58 (s, 1H), 7.45 (d, J = 9.0 Hz, 2H), 6.82 (d, J = 9.0 Hz, 2H), 5.52-5.38 (m, 1H), 3.62-3.44 (m, 1H), 3.03 (s, 6H), 2.29 (dd, J = 13.2, 2.1 Hz, 1H). ^{13}C-NMR (DMSO-d_6) δ 193.39, 172.79, 169.33, 167.33, 152.55, 134.76, 133.71, 120.64, 112.95, 112,90, 55.18, 40.29, 38.00. FTIR - 2922, 1719, 1676, 1563, 1524,

1436, 1412, 1366, 1343, 1283, 1254, 1168, 1104, 1045, 1003, 962, 943, 893, 800, 764 cm^{-1}. HRMS (ESI^+): calcd 381.0573 for $C_{16}H_{17}N_2O_5S_2$ $[M+H]^+$; Found: 381.0578.

(2*S*)-2-[(5*Z*)-5-[4-(Dimethylamino)benzylidene]-4-oxo-2-thioxo-1,3-thiazolidin-3-yl]-3-(1*H*-indol-3-yl)propanoic acid (12). Red solid, 73% yield. M.p. 148-150 °C, from toluene. ^{1}H-NMR (DMSO-d_6) δ 10.77 (s, 1H), 7.62 (s, 1H), 7.48 (d, J = 7.8, Hz, 1H), 7.41 (d, J = 9 Hz, 2H), 7.27 (d, J = 7.8 Hz, 1H), 7.1-6.98 (m, 2H), 6.90 (t, J = 7.8 Hz, 1H), 6.80 (d, J = 9.0 Hz, 2H), 5.96-5.73 (m, 1H), 3.85-3.67 (m, 1H), 3.59 (dd, J = 14.9, 4.9 Hz, 1H), 3.03 (s, 6H). ^{13}C-NMR (DMSO-d_6) δ 192.99, 169.91, 167.30, 152.69, 136.62, 135.56, 133.96, 127.85, 124.25, 121.55, 120.39, 119.01, 118.59, 113.33, 112.91, 112.01, 109.91, 58.66, 40.26, 23.79. FTIR - 3407, 2902, 1690, 1611, 1556, 1517, 1437, 1374, 1340, 1277, 1221, 1165, 1098, 943, 885, 810, 738 cm^{-1}. HRMS (ESI^+): calcd 452.1097 for $C_{23}H_{22}N_3O_3S_2$ $[M+H]^+$; Found: 452.1113.

(2*S*)-4-Methyl-2-[(5*Z*)-5-{[4-(dimethylamino)naphthalene-1-yl]methylidene}-4-oxo-2-thioxo-1,3-thiazolidin-3-yl]pentanoic acid (13). Red solid, 72% yield. M.p. 165-167 °C, from preparative TLC hexane/acetone 4:1. ^{1}H-NMR (DMSO-d_6) δ 8.33 (s, 1H), 8.16 (d, J = 7.8 Hz, 2H), 7.67-7.50 (m, 3H), 7.16 (d, J = 7.8 Hz, 1H), 5.58-5.10 (m, 1H), 2.92 (s, 6H), 2.43-1.27 (m, 3H), 0.88 (d, J = 13.4 Hz, 6H). ^{13}C-NMR (DMSO-d_6) δ 195.21, 167.28, 154.46, 133.63, 129.62, 129.19, 128.2, 127.94, 126.33, 125.93, 124.29, 123.57, 121.66, 121.64, 113.81, 58.75, 45.02, 26.33, 23.93, 22.58. FTIR - 2952, 1695, 1556, 1514, 1386, 1332, 1270, 1200, 1134, 1012, 761, 736 cm^{-1}. HRMS (ESI^+): calcd 429.1301 for $C_{22}H_{25}N_2O_3S_2$ $[M+H]^+$; Found: 429.1313.

(2*R*)-4-Methyl-2-[(5*Z*)-5-{[4-(dimethylamino)naphthalene-1-yl]methylidene}-4-oxo-2-thioxo-1,3-thiazolidin-3-yl]pentanoic acid (14). Red solid, 73% yield. M.p. 152-155 °C, from preparative TLC hexane/acetone 4:1. ^{1}H-NMR (DMSO-d_6) δ 8.32 (s, 1H), 8.15 (d, J = 7.8 Hz, 2H), 7.71-7.40 (m, 3H),

7.14 (d, *J* = 7.8 Hz, 1H), 5.59-5.30 (m, 1H), 2.94 (s, 6H), 2.41-1.27 (m, 3H), 0.88 (d, *J* = 12.5 Hz, 6H). ^{13}C-NMR (DMSO-d_6) δ 195.06, 167.18. 154.59. 133.66, 130.08, 129.32, 128.06, 127.87, 125.94, 126.14, 124.30, 123.42, 121.31, 121.27, 113.76, 58.75, 45.00, 26.02, 23.81, 22.69. FTIR - 2953, 1696, 1554, 1514, 1452, 1387, 1332, 1270, 1199, 1134, 1038, 1012, 909, 854, 761, 736, 687 cm^{-1}. HRMS (ESI$^+$): calcd 429.1301 for $C_{22}H_{25}N_2O_3S_2$ [M+H]$^+$; Found: 429.1300.

(*2R,S*)-2-[(5*Z*)-5-{[4-(Dimethylamino)naphthalene-1-yl]methylidene}-4-oxo-2-thioxo-1,3-thiazolidin-3-yl]pentanoic acid (15). Red solid, 70% yield. M.p. 157-160 °C, from preparative TLC hexane/acetone 4:1. ^{1}H-NMR (DMSO-d_6) δ 8.29 (s, 1H), 8.16 (d, *J* = 7.8 Hz, 2H), 7.72-7.48 (m, 3H), 7.16 (d, *J* = 7.8 Hz, 1H), 5.48-5.10 (m, 1H), 2.92 (s, 6H), 2.42-1.0 (m, 6H), 0.87 (s, 3H). ^{13}C-NMR (DMSO-d_6) δ 195.37, 167.21, 154.36, 133.59, 129.18, 129.09, 128.19, 127.96, 126.35, 125.91, 124.28, 123.68, 121.86, 121.43, 113.84, 61.31, 45.03, 31.27, 20.60, 14.55**.** FTIR - 3391, 2955, 2869, 1698, 1553, 1514, 1452, 1387, 1335, 1268, 1198, 1124, 1096, 1038, 1012, 908, 817, 761, 687 cm^{-1}. HRMS (ESI$^+$): calcd 415.1144 for $C_{21}H_{23}N_2O_3S_2$ [M+H]$^+$; Found: 415.1142.

(*2R,S*)-2-[(5*Z*)-5-{[4-(Dimethylamino)naphthalene-1-yl]methylidene}-4-oxo-2-thioxo-1,3-thiazolidin-3-yl]hexanoic acid (16). Red solid, 70% yield. M.p. 159-163 °C, from preparative TLC hexane/acetone 4:1. ^{1}H-NMR (DMSO-d_6) δ 8.32 (s, 1H), 8.15 (d, *J* = 7.8 Hz, 2H), 7.7-7.52 (m, 3H), 7.15 (d, *J* = 7.8 Hz, 1H), 5.54-5.21 (m, 1H), 2.92 (s, 6H), 2.44-1.81 (m, 2H), 1.46-0.98 (m, 4H), 0.78 (s, 3H). ^{13}C-NMR (DMSO-d_6) δ 195.19, 167.09, 154.51, 133.63, 129.54, 129.08, 128.19, 127.96, 126.14, 125.91, 124.27, 123.48, 121.81, 121.43, 113.77, 60.55, 44.67, 29.51, 29.25, 22.52, 14.10**.** FTIR **-** 2951, 1867, 1697, 1553, 1514, 1452, 1387, 1334, 1221, 1191, 1126, 1039, 1012, 914, 819, 761, 735, 687 , 687 cm^{-1}. HRMS (ESI$^+$): calcd 429.1301 for $C_{22}H_{25}N_2O_3S_2$ [M+H]$^+$; Found: 429.1300.

(2*S*)-3-(1*H*-Indol-3-yl)-2-[(5*Z*)-5-{[4-(dimethylamino)naphthalene-1-yl]methylidene}-4-oxo-2-thioxo-1,3-thiazolidin-3-yl]propanoic acid (17). Red solid, 68% yield. M.p. 189-192 °C, from preparative TLC hexane/acetone 3:1. ^{1}H-NMR ($CDCl_3$) δ 8.39 (s, 1H), 8.21 (d, *J* = 8.7 Hz, 1H), 8.13 (d, *J* = 8.1 Hz, 1H), 7.97 (s, 1H), 7.67-7.45 (m, 4H), 7.30 (d, *J* = 7.8 Hz, 1H), 7.20-6.99 (m, 2H), 6.21-6.05 (m, 1H), 3.95-3.71 (m, 2H), 2.99 (s, 6H). ^{13}C-NMR ($CDCl_3$) δ 193.59, 172.37, 167.19, 154.59, 136.22, 133.81, 130.93, 128.76, 128.28, 127.60, 127.57, 125.74, 125.64, 124.01, 123.97, 123.34, 122.35, 121.24, 119.87, 118.76, 113.12, 111.29, 110.65, 57.63, 44.93, 23.96. FTIR - 3406, 2938, 1698, 1553, 1514, 1455, 1387, 1334, 1275, 1176, 1038, 1012, 734 cm^{-1}. HRMS (ESI^{+}): calcd 502.1253 for $C_{27}H_{24}N_2O_3S_2$ $[M+H]^+$; Found: 502.1254.

{3-Methyl-1-[(5*Z*)-5-{[4-(dimethylamino)naphthalene-1-yl]methylidene}-4-oxo-2-thioxo-1,3-thiazolidin-3-yl]-3-methylbutyl}phosphonic acid (18). Red solid, 65% yield. M.p. 231-233 °C, purified by washing several times with acetone. ^{1}H-NMR (DMSO-d_6) δ 8.35 (s, 1H), 8.21-8.11 (m, 2H), 7.74-7.50 (m, 3H), 7.16 (d, *J* = 8.2 Hz, 1H), 5.46-5.29 (m, 1H), 2.93 (s, 6H), 2.46-1.79 (m, 2H), 1.41-1.1 (m, 4H), 0.81 (t, *J* = 6.9 Hz, 3H). ^{13}C-NMR (DMSO-d_6) δ 194.95, 166.58, 154.63, 133.65, 130.03, 129.29, 128.09, 127.80, 126.17, 126.00, 124.20, 123.35, 120.39, 113.78, 55.79 (d, *J* = 146 Hz), 45.01, 28.54 (d, *J* = 11.2 Hz), 26.93, 22.47, 14.43. FTIR - 2930, 2864, 1698, 1562, 1514, 1451, 1387, 1359, 1319, 1249, 1202, 1125, 1013, 914, 824, 761, 727 cm^{-1}. HRMS (ESI^{+}): calcd 465.1066 for $C_{21}H_{26}N_2O_4PS_2$ $[M+H]^+$; Found: 465.1065.

***N*-{(5*Z*)-5-[4-(Dimethylamino)benzylidene]-4-oxo-2-thioxo-1,3-thiazolidin-3-yl}-3-methylbutanamide (19).** Orange solid, 68% yield. M.p. 250-251 °C, from acetic acid. ^{1}H-NMR (DMSO-d_6) δ 11.00 (s, 1H), 7.71 (s, 1H), 7.46 (d, *J* = 9.1 Hz, 2H), 6.81 (d, *J* = 9.1 Hz, 2H), 3.02 (s, 6H), 2.18 (d, *J* = 6.9 Hz, 2H), 2.12-1.95 (m, 1H), 0.94 (d, *J* = 7.4 Hz, 6H). ^{13}C-NMR (DMSO-d_6) δ 190.84, 170.51, 164.09, 152.80, 136.55, 134.17, 120.35, 112.92, 111.34, 42.81, 26.98, 22.89. FTIR -

3214, 2952, 2869, 1719, 1664, 1612, 1579, 1514, 1435, 1369, 1265, 1242, 1190, 1147, 1112, 988, 947, 807, 711 cm^{-1}. HRMS (ESI^+): calcd 364.1147 for $C_{17}H_{22}N_3O_2S_2$ $[M+H]^+$; Found: 364.1153.

3-{(5*Z*)-5-[4-(Dimethylamino)benzylidene]-4-oxo-2-thioxo-1,3-thiazolidin-3-yl}propanoic acid (20). Red solid, 46% yield. M.p. 260-262 °C, from acetic acid. ^{1}H-NMR (DMSO- d_6) δ 12.50 (s, 1H), 7.64 (s, 1H), 7.43 (d, *J* = 8.9 Hz, 2H), 6.81 (d, *J* = 9.0 Hz, 2H), 4.31-4.10 (m, 2H), 3.04 (s, 6H), 2.70-2.54 (m, 2H). ^{13}C-NMR (DMSO- d_6) δ 193.1, 172.43, 167.33, 152.56, 135.29, 133.85, 120.49, 114.48, 112.85, 40.48, 40.26, 31.55. FTIR - 2894, 1691, 1610, 1561, 1519, 1431, 1360, 1329, 1303, 1262, 1223, 1160, 1092, 1160, 1092, 1064, 947, 810, 794, 739, 668 cm^{-1}. HRMS (ESI^+): calcd. 337.0675 for $C_{15}H_{17}N_2O_3S_2$ $[M+H]^+$; Found: 337.0683.

(2*S*)-2-{(5*Z*)-5-[4-(Diethylamino)benzylidene]-4-oxo-2-thioxo-1,3-thiazolidin-3-yl}-4-methylpentanoic acid (21). Red solid, 70% yield. M.p. 109-110 °C, from preparative TLC hexane/acetone 3:1. ^{1}H-NMR (DMSO-d_6) δ 7.62 (s, 1H), 7.42 (d, *J* = 9.0 Hz, 2H), 6.78 (d, *J* = 9.0 Hz, 2H), 5.63-5.49 (m, 1H), 3.41 (q, *J* = 6.9 Hz, 4H), 2.28-1.89 (m, 2H), 1.52-1.33 (m, 1H), 1.10 (t, *J* = 6.9 Hz, 6H), 0.90 (d, *J* = 6.6 Hz, 3H), 0.87 (d, *J* = 6.6 Hz, 3H) ^{13}C-NMR (DMSO-d_6) δ 193.38, 170.26, 167.30, 150.58, 136.02, 134.47, 119.86, 112.52, 112.51, 56.34, 44.70, 37.18, 25.54, 23.55, 22.68, 13.10. FTIR - 2960, 1695, 1610, 1561, 1515, 1438, 1409, 1338, 1269, 1213, 1183, 1157, 1096, 1074, 811 cm^{-1}. HRMS (ESI^+): calcd 407.1457 for $C_{20}H_{27}N_2O_3S_2$ $[M+H]^+$; Found: 407.1467.

(2*S*)-2-{(5*Z*)-5-[4-(Methylsulfanyl)benzylidene]-4-oxo-2-thioxo-1,3-thiazolidin-3-yl}methyl pentanoic acid (22). Yellow solid, 75% yield. M.p. 79-81 °C, from preparative TLC hexane/acetone 3:1. ^{1}H-NMR (DMSO-d_6) δ 7.78 (s, 1H), 7.56 (d, *J* = 8.6 Hz, 2H), 7.39 (d, *J* = 8.6 Hz, 2H), 5.61-5.48 (m, 1H), 2.52 (s, 3H), 2.24-1.92 (m, 2H), 1.54-1.38 (m, 1H), 0.9 (d, *J* = 6.6 Hz, 3H), 0.84 (d, *J* = 6.6 Hz, 3H). ^{13}C-NMR (DMSO-d_6) δ 193.94, 170.04, 167.28, 144.48, 134.45, 131.92, 129.54, 126.48, 119.93,

56.54, 37.09, 25.50, 23.55, 22.62, 14.64. FTIR - 2957, 1709, 1578, 1491, 1332, 1273, 1238, 1206, 1188, 1137, 1088, 810, 742 cm^{-1}. HRMS (ESI^+): calcd 382.0599 for $C_{17}H_{20}N_1O_3S_3$ $[M+H]^+$; Found: 382.0603.

(2*S*)-2-[(5*Z*)-5-(4-Fluorobenzylidene)-4-oxo-2-thioxo-1,3-thiazolidin-3-yl]-4-methylpentanoic acid (23). Yellow solid, 80% yield. M.p. 72-73 °C, from preparative TLC hexane/acetone 3:1. ^{1}H-NMR (DMSO-d_6) δ 7.82 (s, 1H), 7.75-7.64 (m, 2H), 7.37 (t, *J* = 8.7 Hz, 2H), 5.63-5.46 (m, 1H), 2.25-1.90 (m, 2H), 1.56-1.33 (m, 1H), 0.88 (d, *J* = 6.6 Hz, 3H), 0.83 (d, *J* = 6.6 Hz, 3H). ^{13}C-NMR (DMSO-d_6) δ 194.17, 169.99, 167.20, 164.45 (d, *J* = 250 Hz), 133.99 (d, *J* = 8.8 Hz), 133.48, 130.21 (d, *J* = 3.2 Hz), 121.44, 117.41 (d, *J* = 21.8 Hz), 56.76, 37.12, 25.52, 23.54, 22.59. FTIR - 3541, 2958, 1696, 1592, 1505, 1468, 1410, 1336, 1279, 1226, 1197, 1158, 1108, 1022, 918, 826, 742 cm^{-1}. HRMS (ESI^+): calcd 354.0628 for $C_{16}H_{17}FNO_3S_2$ $[M+H]^+$; Found: 354.0629.

(2*S*)-2-{(5*Z*)-5-[4-(Diethylamino)benzylidene]-4-oxo-2-thioxo-1,3-thiazolidin-3-yl]-3-(1*H*-indol-3-yl)propanoic acid (24). Red solid, 74 % yield. M.p. 198-201 °C, from preparative TLC hexane/acetone 4:1. ^{1}H-NMR (DMSO-d_6) δ 10.88 (s, 1H), 7.66 (d, *J* = 7.2 Hz, 1H), 7.64 (s, 1H), 7.43 (d, *J* = 9.0 Hz, 2H), 7.33 (d, *J* = 7.9 Hz, 1H), 7.20 (d, *J* = 2.1 Hz, 1H), 7.10-6.95 (m, 2H), 6.79 (d, *J* = 9.0 Hz, 2H), 4.34-4.16 (m, 2H), 3.42 (q, *J* = 6.8 Hz, 4H), 3.11-2.95 (m, 2H), 1.11 (t, *J* = 7.0 Hz, 6H). ^{13}C-NMR (DMSO-d_6) δ 193.12, 174.70, 169.97, 167.45, 150.37, 136.63, 135.15, 134.29, 129.58, 128.89, 127.92, 124.10, 121.50, 119.90, 119.11, 112.25 112.23, 110.50, 59.50, 44.67, 23.82, 13.11. FTIR - 3406, 2970, 1699, 1562, 1515, 1340, 1271, 1221, 1176, 1099, 1010, 812, 738 cm^{-1}. HRMS (ESI^+): calcd 480.1410 for $C_{25}H_{26}N_3O_2S_2$ $[M+H]^+$; Found: 480.1418.

(2*S*)-2-[(5*Z*)-5-(4-Propylbenzylidene-4-oxo-2-thioxo-1,3-thiazolidin-3-yl]-3-(1*H*-indol-3-yl)propanoic acid (25). Yellow solid, 83% yield. M.p. 146-148 °C, from preparative TLC hex-

ane/acetone 4:1. ^{1}H-NMR (DMSO-d_6) δ 10.75 (s, 1H), 7.73 (s, 1H), 7.48 (d, J = 7.5 Hz, 1H), 7.49 (s, 1H), 7.41-7.17 (m, 3H), 7.14-6.78 (m, 4H), 5.90-5.75 (m, 1H), 3.87-3.57 (m, 2H), 2.58 (t, J = 7.5 Hz, 2H), 1.66-1.44 (m, 2H), 0.86 (t, J = 7.2 Hz, 3H). ^{13}C-NMR (DMSO-d_6) δ 193.63, 169.92, 167.30, 146.83, 136.64, 134.14, 131.53, 131.06, 130.23, 127.82, 124.23, 121.57, 120.63, 119.02, 118.58, 112.05, 110.11, 59.39, 37.83, 24.42, 23.90, 14.31. FTIR - 3402, 2928, 1750, 1592, 1451, 1338, 1278, 1238, 1177, 1115, 869, 738 cm^{-1}. HRMS (ESI^{+}): calcd 451.1144 for $C_{24}H_{23}N_2O_3S_2$ [M+H]$^{+}$; Found: 451.1143.

(2*S*)-2-[(5*Z*)-5-{4-[bis(2-Chloroethyl)amino]benzylidene-4-oxo-2-thioxo-1,3-thiazolidin-3-yl]-3-(1*H*-indol-3-yl)propanoic acid (26). Red solid, 82% yield. M.p. 172-174 °C, from preparative TLC DCM/MeOH 5:1. ^{1}H-NMR (DMSO-d_6) δ 10.66 (s, 1H), 7.55 (s, 1H), 7.46-7.35 (m, 3H), 7.23 (d, J = 7.8 Hz, 1H), 7.01-6.84 (m, 5H), 5.72-5.57 (m, 1H), 4.33-4.03 (m, 2H), 3.85-3.55 (m, 8H). ^{13}C-NMR (DMSO-d_6) δ 193.75, 170.96, 167.72, 149.58, 136.66, 136.50 133.81, 127.98, 123.48, 121.95, 121.65, 121.45, 118.84, 118.68, 113.22, 113.16, 111.96, 61.44, 52.33, 41.62, 21.34. FTIR - 3396, 2968, 1698, 1567, 1514, 1395, 1342, 1275, 1224, 1170, 1101, 948, 813, 740 cm^{-1}. HRMS (ESI^{-}): calcd 546.0485 for $C_{25}H_{22}Cl_2N_3O_3S_2$ [M-H]$^{-}$. Found: 546.0473.

(2*R*)-2-[(5*Z*)-4-Oxo-5-(4-propylbenzylidene-4-oxo-2-thioxo-1,3-thiazolidin-3-yl]-3-(1*H*-indol-3-yl)propanoic acid (27). Yellow solid, 81% yield. M.p. 165-167 °C, from preparative TLC hexane/acetone 4:1. ^{1}H-NMR (DMSO-d_6) δ 10.79 (s, 1H), 7.71 (s, 1H), 7.48 (d, J = 7.4 Hz, 1H), 7.46 (s, 1H), 7.41-7.15 (m, 3H), 7.11-6.79 (m, 4H), 5.90-5.77 (m, 1H), 3.91-3.62 (m, 2H), 2.57 (t, J = 7.4 Hz, 2H), 1.64-1.47 (m, 2H), 0.86 (t, J = 7.2 Hz, 3H). ^{13}C-NMR (DMSO-d_6) δ 193.80, 169.88, 167.36, 146.73, 136.66, 133.89, 131.30, 130.21, 127.86, 124.08, 121.54, 120.78, 118.98, 118.6, 112.04, 110.45, 59.99, 37.83, 24.41, 24.05, 14.31. FTIR - 3407 2958, 1704, 1591, 1455, 1338, 1277, 1237, 1177, 1115, 870, 737 cm^{-1}. HRMS (ESI^{+}): calcd 451.1144 for $C_{24}H_{23}N_2O_3S_2$ [M+H]$^{+}$; Found: 451.1145.

(2*R*)-2-[(5*Z*)-5-{4-[bis(2-Chloroethyl)amino]benzylidene-4-oxo-2-thioxo-1,3-thiazolidin-3-yl]-3-(1*H*-indol-3-yl)propanoic acid (28). Red solid, 80% yield. M.p. 181-184 °C, from preparative TLC DCM/MeOH 5:1. ^{1}H-NMR (DMSO-d_6) δ 10.69 (s, 1H), 7.58 (s, 1H), 7.48-7.35 (m, 3H), 7.24 (d, J = 8.0 Hz, 1H), 7.01-6.81 (m, 5H), 5.79-5.62 (m, 1H), 4.20-3.96 (m, 2H), 3.88-3.53 (m, 8H). ^{13}C-NMR (DMSO-d_6) δ 193.35, 170.79, 167.28, 149.51, 136.49, 136.44, 133.68, 127.73, 123.57, 121.68, 121.39, 121.27, 118.70, 118.42, 113.04, 112.97, 111.76, 61.38, 52.14, 41.41 21.11. FTIR - 3400, 2912, 1698, 1566, 1513, 1456, 1395, 1340, 1276, 1222, 1170, 1101, 1036, 812, 739 cm^{-1}. HRMS (ESI$^-$): calcd `546.0485 for $C_{25}H_{22}Cl_2N_3O_3S_2$ [M-H]$^-$. Found: 546.0472.

(2*S*)-2-[(5*Z*)-5-(4-Chlorobenzylidene)-4-oxo-2-thioxo-1,3-thiazolidin-3-yl]-3-(1*H*-indol-3-yl)propanoic acid (29). Yellow solid, 83% yield M.p. 181-183 °C, from preparative TLC hexane/acetone 3:1. ^{1}H-NMR (DMSO-d_6) δ 10.79 (s, 1H), 7.78 (s, 1H), 7.6-7.56 (m, 2H), 7.54-7.34 (m, 2H), 7.33-7.15 (m, 2H), 7.14-6.8 (m, 4H), 5.93-5.72 (m, 1H), 3.91-3.59 (m, 2H). ^{13}C-NMR (DMSO-d_6) δ 193.47, 169.86, 167.18, 136.65, 136.39, 132.95, 132.54, 132.36, 130.23, 129.18, 127.82, 124.21, 122.57, 121.58, 119.24, 119.03, 118.57, 112.05, 67.03. FTIR - 3398, 2914, 1710, 1610, 1591, 1489, 1456, 1339, 1279, 1236, 1177, 1116, 1090, 1010, 869, 821, 738 cm^{-1}. HRMS (ESI$^-$): calcd. 441.0139 for $C_{21}H_{14}ClN_2O_3S_2$ [M-H]$^-$. Found: 441.0153.

(2*S*)-2-[(5*Z*)-5-(2,4-Dichlorobenzylidene)-4-oxo-2-thioxo-1,3-thiazolidin-3-yl]-3-(1*H*-indol-3-yl)propanoic acid (30). Yellow solid, 81% yield. M.p. 167-169 °C, from preparative TLC hexane/acetone 3:1. ^{1}H-NMR (DMSO-d_6) δ 10.78 (s, 1H), 7.87 (s, 1H), 7.82-7.63 (m, 1H), 7.62-7.55 (m, 1H), 7.39-7.40 (m, 2H), 7.38-7.20 (m, 2H), 7.12-6.86 (m, 3H), 5.88-5.64 (m, 1H), 3.86-3.59 (m, 2H). ^{13}C-NMR (DMSO-d_6) δ 193.38, 169.67, 166.96, 136.66, 136.36, 131.25, 130.84, 130.71, 130.42, 129.14, 127.83, 124.07, 118.98, 118.57, 112.03, 111.95, 110.64, 110.57, 67.03. FTIR - 3399, 2915,

1713, 1579, 1456, 1339, 1235, 1105, 1047, 869, 739 cm^{-1}. HRMS (ESI^-): calcd. 474.9750 for $C_{21}H_{14}ClN_2O_3S_2$ $[M-H]^-$; Found: 474.9750.

(5*Z*)-5-[4-(Diethylamino)benzylidene]-3-[2-(1*H*-indol-3-yl)ethyl]-2-thioxo-1,3-thiazolidin-4-one (31). Red solid, 80% yield. M.p. 196-198 °C, from acetic acid. ^{1}H-NMR (DMSO-d_6) δ 10.88 (s, 1H), 7.72-7.60 (m, 2H), 7.44 (d, J = 9.1 Hz, 2H), 7.33 (d, J = 7.9 Hz, 1H), 7.21 (d, J = 2.3 Hz, 1H), 7.13-6.93 (m, 2H), 6.81 (d, J = 9.1 Hz, 2H), 4.35-4.18 (m, 2H), 3.43 (q, J = 6.9, 4H), 3.10-2.97 (m, 2H), 1.11 (t, J = 7.2 Hz, 6H). ^{13}C-NMR (DMSO-d_6) δ 193.06, 167.51, 150.32, 136.97, 135.23, 134.28, 127.77, 123.78, 121.77, 119.98, 119.14, 118.92, 114.01, 112.42,112.18, 110.80, 45.36, 44.66, 23.21, 13.09. FTIR 3367, 2967, 1682, 1610, 1560, 1517, 1411, 1377, 1350, 1326, 1270, 1240, 1193, 1166, 1097, 1077, 1010, 810, 735 cm^{-1}. HRMS (ESI^+): calcd 436.1511 for $C_{24}H_{26}N_3OS_2$ $[M+H]^+$; Found: 436.1512.

(2*S*)-2-{(5*Z*)-5-[(10-Chloroanthracen-9-yl)methylidene-4-oxo-2-thioxo-1,3-thiazolidin-3-yl]-3-(1*H*-indol-3-yl)propanoic acid (32). Yellow solid, 83% yield. M.p. 165-167 °C, from preparative TLC hexane/acetone 4:1. ^{1}H-NMR (DMSO-d_6) δ 10.90 (s, 1H), 8.53 (s, 1H), 8.43 (d, J = 8.6 Hz, 2H), 7.85-7.58 (m, 6H), 7.52 (d, J = 7.8 Hz, 1H), 7.35 (d, J = 8.3 Hz, 1H), 7.22 - 6.95(m, 3H), 5.87-5.78 (m, 1H), 3.79-3.56 (m, 2H). ^{13}C-NMR (DMSO-d_6) δ 193.40, 169.65, 165.40, 136.63, 131.71, 131.39, 130.82, 128.72, 128.58, 128.35, 128.27, 127.98,127.80, 126.12, 125.51, 125.05, 121.53, 119.28, 118.24, 112.22, 109.62, 59.58, 31.37, 23.68. FTIR - 3411, 2899, 1707, 1597, 1438, 1341, 1223, 1174, 933, 732 cm^{-1}. HRMS (ESI^+): calcd 543.0598 for $C_{29}H_{20}ClN_2O_3S_2$ $[M+H]^+$; Found: 543.0596.

(2*S*)-2-{(5*Z*)-5-[(4-Methylnaphthalen-1-yl)methylidene-4-oxo-2-thioxo-1,3-thiazolidin-3-yl]-3-(1*H*-indol-3-yl)propanoic acid (33). Yellow solid, 84% yield. M.p. 143-145 °C, from preparative TLC hexane/acetone 4:1. ^{1}H-NMR (DMSO-d_6) δ 10.80 (s, 1H), 8.38 (s, 1H), 8.23-8.05 (m, 2H), 7.74- 7.60

(m, 2H), 7.56-7.40 (m, 2H), 7.27 (d, *J* = 8.2 Hz, 1H), 7.16-6.82 (m, 3H), 5.97-5.73 (m, 1H), 3.87-3.47 (m, 2H), 2.67 (s, 3H). ^{13}C-NMR (DMSO-d_6) δ 194.24, 174.65, 166.70, 139.46, 136.65, 132.97, 131.73, 130.97, 128.88, 128.11, 127.85, 127.75, 127.60, 127.19, 125.79, 124.59, 124.39, 124.19, 121.55, 119.05, 118.56, 112.04, 110.09, 62.56, 26.18, 20.19. FTIR - 3410, 2969, 1703, 1590, 1564, 1514, 1456, 1337, 1277, 1227, 1176, 1119, 1033, 943, 813, 734 cm^{-1}. HRMS (ESI$^+$): calcd 473.0988 for $C_{26}H_{21}N_2O_3S_2$ [M+H]$^+$; Found: 473.0978.

(2*R*)-2-{(5*Z*)-5-[(4-Methylnaphthalen-1-yl)methylidene-4-oxo-2-thioxo-1,3-thiazolidin-3-yl]-3-(1*H*-indol-3-yl)propanoic acid (34). Yellow solid, 83% yield. M.p. 138-140 °C, from preparative TLC hexane/acetone 4:1. ^{1}H-NMR (DMSO-d_6) δ 10.82 (s, 1H), 8.37 (s, 1H), 8.18-7.99 (m, 2H), 7.72-7.60 (m, 2H), 7.56-7.39 (m, 3H), 7.27 (d, *J* = 8 Hz, 1H), 7.16-6.85 (m, 3H), 6.01-5.84 (m, 1H), 3.85-3.58 (m, 2H), 2.66 (s, 3H). ^{13}C-NMR (DMSO-d_6) δ 194.10, 169.75, 166.66, 139.53, 136.66, 132.95, 131.72, 131.18, 128.79, 128.09, 127.85, 127.75, 127.60, 127.19, 125.76, 124.57, 124.39, 123.95, 121.60, 119.11, 118.56, 112.07, 109.71, 58.94, 23.83, 20.19. FTIR - 3404, 2894, 1705, 1590, 1563, 1335, 1279, 1251, 1178, 1033, 815, 734 cm^{-1}. HRMS (ESI$^+$): calcd 473.0988 for $C_{26}H_{21}N_2O_3S_2$ [M+H]$^+$; Found: 473.0991.

All the target compounds **1-34** were obtained in good yields and characterized by the means of IR, ^{1}H, ^{13}C NMR and HRMS.

Expression and Purification of *Mtb* InhA

Mtb InhA was expressed in *E. coli* strain Rosetta(DE3)pLysS using the InhA expression plasmid kindly provided by Prof. Dr. Caroline Kisker (University of Würzburg, Germany) and purified following a slightly modified protocol published recently.[28] Briefly, a 1 liter culture of TB was inoculated over night for 14h at 37°C before reducing the temperature to 25°C. Then expression was induced with 1

mM IPTG and cells were harvested by centrifugation after 24h. The collected bacteria were suspended in purification buffer (20 mM Tris/HCl, 500 mM NaCl, 20 mM imidazole, pH 8.0) and supplemented with a small amount of DNase before passing the suspension twice through a French Press. The crude extract was clarified by centrifugation (20 min, 4°C, 9800 rpm) before it was applied onto a 5 ml Ni-chelating column and subsequently eluted with a gradient of 20-500 mM imidazole (for 20 CV). Fractions containing InhA were pooled, concentrated and further purified via a Superdex 200 column (GE Healthcare) equilibrated with gel filtration buffer (30 mM Pipes, 150 mM NaCl, 1 mM EDTA), affording highly pure (>95%) and active InhA as judged by SDS-PAGE (Coomassie stained) and activity assay, respectively.

Mtb InhA Inhibition Assay

Mtb InhA was assayed using a spectrophotometric method at 25 °C by monitoring the initial velocities (120 seconds) of the decrease in the absorbance of NADH at 340 nm in presence of the substrate *trans*-2-decenoyl-N-acetylcysteamine, which was synthesized from *trans*-2-decenoic acid and N-acetylcysteamine using the mixed anhydride method as described previously.[29] The standard reaction mixture, in a total volume of 1.0 mL, consisted of assay buffer (30 mM PIPES, 150 mM NaCl, 1 mM EDTA, pH 6.8), 200 μM *trans*-2-decenoyl-N-acetylcysteamine, 100 μM NADH, and 1 µg of purified recombinant *Mtb* InhA. For initial screening, the compounds were dissolved in DMSO to obtain stock solutions at a concentration of 30 mM. IC_{50} values were determined at increasing inhibitor concentrations and subsequently calculated by nonlinear fit to the sigmoidal dose-response curve using Prism 6.0 (GraphPad Software, San Diego, CA, USA). Triclosan was used as positive control and provided an IC_{50} of 6.1 ± 2.1 μM which is close to values reported in the literature.[7a] All assays were performed in triplicates with DMSO fixed at a concentration of 0.1%.

Molecular Modeling

The model of apo InhA was constructed by removing all water molecules and ligands from the X-ray structure (PDBcode: 1P45),[30] and by adding the Hydrogen atoms using SYBYL-X 2.1.1 (Tripos Associates Inc, USA).[31] We selected the chain A of the PDB structure 1P45, which shows the peculiarity to present two molecules of Triclosan in complex with the active site of InhA. This gave us the opportunity to explore a higher volume of the InhA binding side together with a highly diverse and larger chemical space in the active site of the InhA, and then search for additional interactions, especially in the hydrophobic pocket, together with those "more classical" ones established with Tyr158 and NAD+. The 3D models of the ligands were built by using the Maestro program, a tool from the Schrödinger 2013 package.[32] Refinement and energy minimization of ligands were carried out by using the OPLS-2005 forcefield and 10.000 iterations. Docking simulations were carried out by means of GOLD, 5.2.2 version.[23] GOLD 5.2.2 adopts a search genetic algorithm to generate lowest binding ligand-protein complex energies. Genetic algorithm default parameters were set: the population size was 100, the selection pressure was 1.1, the number of operations was 10^5, the number of islands was 5, the niche size was 2, migrate was 10, mutate was 95, and crossover was 95. Docking calculations were computed to obtain 100 randomly seeded runs for each ligand. Binding-site cavity was set as a spherical region of 15 Å radius centred on the phenolic Oxygen atom of Tyr158. To evaluate the single poses resulted by search algorithm GoldScore scoring function was used.

Serial Dilution Test and Determination of MIC Values Against *Mm*

Mm, the laboratory strain mimicking perfectly *Mtb,* were cultivated in a shaking culture at 32°C up to an OD_{600} of 0.8-1 in 7H9 medium supplemented with OADC. 10^5 bacteria were placed into each well of a 96-well white plate containing compounds in 7H9 medium (0.5% v/v DMSO). Bacterial growth at 32°C was monitored by measuring the luminescence in a platereader (Synergy H1) for 48 hours. Amikacin was added as a control at 10 μM concentration. LuxABCDE-expressing *Mm*[33] were transferred

into each well of 96-well white plates containing compounds in 7H9 medium (0.5% v/v DMSO). Bacterial growth at 32°C was monitored by measuring the luminescence in a platereader (Synergy H1) for 48 hours. Amikacin was added as a control at 10 μM concentration.

MIC was determined as the lowest concentration giving a significant signal reduction from the DMSO control after 48 hours of growth.

Mm Virulence Measurement

The assay to measure bacterial virulence relies on the ability of *Dictyostelium* to feed on non-pathogenic bacteria and form phagocytic plaques in the bacterial lawn. In this assay, virulent bacteria including *Mm* do not allow the growth of *Dictyostelium*. The addition of chemical compounds that block bacterial virulence should restore growth of amoebae and formation of phagocytic plaques.

Dictyostelium cells were grown on a mixed bacterial lawn of *Kp* for feeding amoebae and *Mm*. First, a bacterial pellet from one volume of centrifuged mid-log phase mycobacterial cultures was resuspended in an equal volume of an overnight culture of non-virulent *Kp* diluted at 10^{-5} times. Then, 50 μl of the bacterial suspension were plated on 2 mL of solid SM agar medium in 24-well plate format containing the compounds that need to be tested and left to dry for 2-3 hours. Finally, 10^3 *Dictyostelium* cells were added on top of the bacterial lawn. Plates were incubated for 5-9 days at 25 C and the formation of phagocytic plaque was monitored using DMSO as control. Compounds were recorded with scores 0, 1, 2, 3 and 4 according to the diameter of the phagocytic plaque formed following exposure to rhodanine derivatives.

Antibiotic and Infection Assays Against *Lp*

Antibiotic and infection assays against *Lp* were performed according to method described in the literature.[27] *Acanthamoeba castellanii* were cultured in PYG medium[34] and split the day prior to infection such that 2×10^4 cells were present in each well of a 96-well plate (Cell Carrier, black, transparent bot-

tom from Perkin-Elmer). Cultures of *Lp* harbouring the GFP-producing plasmid pNT-28[35] were resuspended from plate to a starting OD_{600} of 0.1 in AYE medium, and grown overnight on a rotating wheel at 37°C to an OD_{600} of 3. Bacteria were diluted in LoFlo medium (ForMedium) such that each well contained 8×10^5 bacteria (MOI 20). Infections were synchronised by centrifugation at 1500 rpm for 10 min. Compounds were added to at least triplicate wells during or after infection depending on the susceptibility time frame being assessed (see Data Analysis for more details). Infected cultures were incubated at 30°C, and the GFP fluorescence was measured by a plate spectrophotometer at appropriate intervals (Optima FluoStar, BMG Labtech). Time courses were constructed and data was used to determine the effect of compounds versus vehicle control. All the data were normalised between 0 (kanamycin treatment: no replication) and 1 (DMSO vehicle control: normal replication).

Serial Dilution Test and Determination of MIC Values Against *Ef* and *Pa*

The bacterial reference strains used in this assay are *Pseudomonas aeruginosa* ATCC 27853 (Pa) and *Efnterococcus faecalis* ATCC 29212 (*Ef*). Mueller-Hinton broth (MHB, Oxoid) and agar (MHA, Biomérieux) were used as liquid and solid medium, respectively. The MICs of the different rhodanine synthetic derivatives were determined by using the broth dilution method in 96-well microtiter plates as previously described.[36] Briefly, compounds were resuspended at 2 mg/ml in DMSO and serially diluted in MHB. 100 µl of doubling dilutions series were dispensed into a 96-well microplate, 100 µl of bacterial inoculum was then added to each well (final concentration of $1\text{-}5 \times 10^5$). All multiplates were incubated at 37°C for 24h Sterility control (medium without inoculum), growth control (bacteria without compounds) and solvent control (DMSO diluted in the medium) were performed. The MIC corresponds to the lowest concentration of the compounds that inhibit visible growth (visual turbidity). The growth was detected by the reduction of p-iodonitrotetrazolium violet (INT, Sigma-Aldrich) into formazan.[37] To this end, 20 µl INTsolution (2 mg/ml) was incubated for several hours. The largest dilution of a compound in which no red-purple color appears corresponds to its MIC (cfu/ml).

ABBREVIATIONS USED

FAS-II - Fatty acid synthase type II; InhA - Mycobacterial enoyl-acyl carrier protein reductase; MIC - minimal inhibitory concentration; *Mm* - *Mycobacterium marinum*, *Mtb* - *Mycobacterium tuberculosis*, *Pa* - *Pseudomonas aeruginosa*, *Lp* - *Legionella pneumophila*, *Ef* - *Enterococcus faecalis*, *Kp* - *Klebsiella pneumoniae*.

Supporting Information

Supporting Information Available: experimental details are reported including: IC_{50} curve of triclosan towards *Mtb* InhA; the inhibitory activity and IC_{50} values of derivatives **1-34** towards *Mtb* InhA; *in vitro* antibacterial activity values of compounds **1-34**; HPLC analyses of the newly synthesized compounds here described.

AUTHOR INFORMATION

[†]These authors contributed equally

*Author correspondence to Prof. Leonardo Scapozza: +41223793363 and leonardo.scapozza@unige.ch

ACKNOWLEDGEMENTS

The authors acknowledge the Swiss National Science Foundation (SNSF) and the University of Geneva for the financial support ("Sinergia" grant CRSI_130016 awarded to L.S., P.C., T.S., H. H.). The Sciex-NMSch grant (code: 10.012) supported L. Slepikas. The authors thank Mr. I. Patmanidis and Ms. S. Mosad for their valuable scientific contribution, Ms. Elinam Gayi, Mr. S. Epsy and Mr. B. Kiening for

their technical assistance. We are indebted to Prof. Dr. Caroline Kisker, University of Würzburg, for providing the InhA expression plasmid.

REFERENCES

1. World Health Organization.; World Health Organization., *Antimicrobial resistance: global report on surveillance.(In IRIS)*. World Health Organization: Geneva, 2014; p xxii, 232 p.
2. Goldberg, D. E.; Siliciano, R. F.; Jacobs, W. R., Jr. Outwitting evolution: fighting drug-resistant TB, malaria, and HIV. *Cell* **2012**, *148*, 1271-1283.
3. Zhang, Y. M.; Lu, Y. J.; Rock, C. O. The reductase steps of the type II fatty acid synthase as anti-microbial targets. *Lipids* **2004**, *39*, 1055-1060.
4. Rawat, R.; Whitty, A.; Tonge, P. J. The isoniazid-NAD adduct is a slow, tight-binding inhibitor of InhA, the Mycobacterium tuberculosis enoyl reductase: adduct affinity and drug resistance. *Proc. Natl. Acad. Sci. U. S. A.* **2003**, *100*, 13881-13886.
5. Ando, H.; Miyoshi-Akiyama, T.; Watanabe, S.; Kirikae, T. A silent mutation in mabA confers iso-niazid resistance on Mycobacterium tuberculosis. *Mol: Microbiol.* **2014**, *91*, 538-547.
6. Cade, C. E.; Dlouhy, A. C.; Medzihradszky, K. F.; Salas-Castillo, S. P.; Ghiladi, R. A. Isoniazid-resistance conferring mutations in Mycobacterium tuberculosis KatG: catalase, peroxidase, and INH-NADH adduct formation activities. *Protein Sci.* **2010**, *19*, 458-474.
7. (a) Sullivan, T. J.; Truglio, J. J.; Boyne, M. E.; Novichenok, P.; Zhang, X.; Stratton, C. F.; Li, H. J.; Kaur, T.; Amin, A.; Johnson, F.; Slayden, R. A.; Kisker, C.; Tonge, P. J. High affinity InhA inhibi-tors with activity against drug-resistant strains of Mycobacterium tuberculosis. *ACS Chem. Biol.* **2006**, *1*, 43-53; (b) Kinjo, T.; Koseki, Y.; Kobayashi, M.; Yamada, A.; Morita, K.; Yamaguchi, K.; Tsurusawa, R.; Gulten, G.; Komatsu, H.; Sakamoto, H.; Sacchettini, J. C.; Kitamura, M.; Aoki, S. Identification of compounds with potential antibacterial activity against Mycobacterium through structure-based drug screening. *J. Chem. Inf. Model.* **2013**, *53*, 1200-1212.

8. He, X.; Alian, A.; Stroud, R.; Ortiz de Montellano, P. R. Pyrrolidine carboxamides as a novel class of inhibitors of enoyl acyl carrier protein reductase from Mycobacterium tuberculosis. *J. Med. Chem.* **2006**, *49*, 6308-6323.

9. (a) Broussy, S.; Bernardes-Genisson, V.; Quemard, A.; Meunier, B.; Bernadou, J. The first chemical synthesis of the core structure of the benzoylhydrazine-NAD adduct, a competitive inhibitor of the Mycobacterium tuberculosis enoyl reductase. *J. Org. Chem* **2005**, *70*, 10502-10510; (b) Delaine, T.; Bernardes-Genisson, V.; Meunier, B.; Bernadou, J. Synthesis of the isonicotinoylnicotinamide scaffolds of the naturally occurring isoniazid-NAD(P) adducts. *J. Org. Chem* **2007**, *72*, 675-678.

10. Hartkoorn, R. C.; Sala, C.; Neres, J.; Pojer, F.; Magnet, S.; Mukherjee, R.; Uplekar, S.; Boy-Rottger, S.; Altmann, K. H.; Cole, S. T. Towards a new tuberculosis drug: pyridomycin - nature's isoniazid. *EMBO Mol. Med.* **2012**, *4*, 1032-1042.

11. Horlacher, O. P.; Hartkoorn, R. C.; Cole, S. T.; Altmann, K. H. Synthesis and antimycobacterial activity of 2,1'-dihydropyridomycins. *ACS Med. Chem. Lett.* **2013**, *4*, 264-268.

12. Carlson, E. E.; May, J. F.; Kiessling, L. L. Chemical probes of UDP-galactopyranose mutase. *Chem. Biol.* **2006**, *13*, 825-837.

13. Sim, M. M.; Ng, S. B.; Buss, A. D.; Crasta, S. C.; Goh, K. L.; Lee, S. K. Benzylidene rhodanines as novel inhibitors of UDP-N-acetylmuramate/L-alanine ligase. *Bioorg. Med. Chem. Lett.* **2002**, *12* (4), 697-699.

14. Hu, Y.; Helm, J. S.; Chen, L.; Ginsberg, C.; Gross, B.; Kraybill, B.; Tiyanont, K.; Fang, X.; Wu, T.; Walker, S. Identification of selective inhibitors for the glycosyltransferase MurG via high-throughput screening. *Chem. Biol.* **2004**, *11*, 703-711.

15. Zervosen, A.; Lu, W. P.; Chen, Z.; White, R. E.; Demuth, T. P., Jr.; Frere, J. M. Interactions between penicillin-binding proteins (PBPs) and two novel classes of PBP inhibitors, arylalkylidene

rhodanines and arylalkylidene iminothiazolidin-4-ones. *Antimicrob. Agents Chemother.* **2004**, *48*, 961-969.

16. Grant, E. B.; Guiadeen, D.; Baum, E. Z.; Foleno, B. D.; Jin, H.; Montenegro, D. A.; Nelson, E. A.; Bush, K.; Hlasta, D. J. The synthesis and SAR of rhodanines as novel class C beta-lactamase inhibitors. *Bioorg. Med. Chem. Lett.* **2000**, *10*, 2179-2182.
17. Mariner, K. R.; Trowbridge, R.; Agarwal, A. K.; Miller, K.; O'Neill, A. J.; Fishwick, C. W.; Chopra, I. Furanyl-rhodanines are unattractive drug candidates for development as inhibitors of bacterial RNA polymerase. *Antimicrob. Agents Chemother.* **2010**, *54*, 4506-4509.
18. Shi, S.; Ehrt, S. Dihydrolipoamide acyltransferase is critical for Mycobacterium tuberculosis pathogenesis. *Infect. Immun.* **2006**, *74*, 56-63.
19. Johnson, S. L.; Jung, D.; Forino, M.; Chen, Y.; Satterthwait, A.; Rozanov, D. V.; Strongin, A. Y.; Pellecchia, M. Anthrax lethal factor protease inhibitors: synthesis, SAR, and structure-based 3D QSAR studies. *J. Med. Chem.* **2006**, *49*, 27-30.
20. Johnson, S. L.; Chen, L. H.; Harbach, R.; Sabet, M.; Savinov, A.; Cotton, N. J.; Strongin, A.; Guiney, D.; Pellecchia, M. Rhodanine derivatives as selective protease inhibitors against bacterial toxins. *Chem. Biol. Drug Des.* **2008**, *71*, 131-139.
21. Ge, X.; Wakim, B.; Sem, D. S. Chemical proteomics-based drug design: target and antitarget fishing with a catechol-rhodanine privileged scaffold for NAD(P)(H) binding proteins. *J. Med. Chem.* **2008**, *51*, 4571-4580.
22. Kumar, G.; Parasuraman, P.; Sharma, S. K.; Banerjee, T.; Karmodiya, K.; Surolia, N.; Surolia, A. Discovery of a rhodanine class of compounds as inhibitors of Plasmodium falciparum enoyl-acyl carrier protein reductase. *J. Med. Chem.* **2007**, *50*, 2665-2675.
23. Cambridge Crystallographic Data Centre. In *http://www.ccdc.cam.ac.uk/Solutions/GoldSuite/pages/GoldSuite.aspx*.

24. Song, M. X.; Zheng, C. J.; Deng, X. Q.; Wang, Q.; Hou, S. P.; Liu, T. T.; Xing, X. L.; Piao, H. R. Synthesis and bioactivity evaluation of rhodanine derivatives as potential anti-bacterial agents. *Eur. J. Med. Chem.* **2012**, *54*, 403-412.

25. Froquet, R.; Lelong, E.; Marchetti, A.; Cosson, P. Dictyostelium discoideum: a model host to measure bacterial virulence. *Nat. Protoc.* **2009**, *4*, 25-30.

26. Reich-Slotky, R.; Kabbash, C. A.; Della-Latta, P.; Blanchard, J. S.; Feinmark, S. J.; Freeman, S.; Kaplan, G.; Shuman, H. A.; Silverstein, S. C. Gemfibrozil inhibits Legionella pneumophila and Mycobacterium tuberculosis enoyl coenzyme A reductases and blocks intracellular growth of these bacteria in macrophages. *J. Bacteriol.* **2009**, *191*, 5262-5271.

27. Harrison, C. F.; Kicka, S.; Trofimov, V.; Berschl, K.; Ouertatani-Sakouhi, H.; Ackermann, N.; Hedberg, C.; Cosson, P.; Soldati, T.; Hilbi, H. Exploring anti-bacterial compounds against intracellular Legionella. *PloS One* **2013**, *8*, e74813.

28. Luckner, S. R.; Liu, N.; Am Ende, C. W.; Tonge, P. J.; Kisker, C. A slow, tight binding inhibitor of InhA, the enoyl-acyl carrier protein reductase from Mycobacterium tuberculosis. *J. Biol. Chem.* **2010**, *285*, 14330-14337.

29. Parikh, S.; Moynihan, D. P.; Xiao, G.; Tonge, P. J. Roles of tyrosine 158 and lysine 165 in the catalytic mechanism of InhA, the enoyl-ACP reductase from Mycobacterium tuberculosis. *Biochemistry* **1999**, *38*, 13623-13634.

30. Kuo, M. R.; Morbidoni, H. R.; Alland, D.; Sneddon, S. F.; Gourlie, B. B.; Staveski, M. M.; Leonard, M.; Gregory, J. S.; Janjigian, A. D.; Yee, C.; Musser, J. M.; Kreiswirth, B.; Iwamoto, H.; Perozzo, R.; Jacobs, W. R., Jr.; Sacchettini, J. C.; Fidock, D. A. Targeting tuberculosis and malaria through inhibition of Enoyl reductase: compound activity and structural data. *J. Biol. Chem.* **2003**, *278* , 20851-20859.

31. SYBYL-X 2.1.1, Tripos International, 1699 South Hanley Rd., St. Louis, Missouri, 63144, USA). In *http://www.certara.com/*.

32. Schrödinger Inc. Cambridge, MA 02142. In www.Schrodinger.com.

33. Andreu, N.; Zelmer, A.; Sampson, S. L.; Ikeh, M.; Bancroft, G. J.; Schaible, U. E.; Wiles, S.; Robertson, B. D. Rapid in vivo assessment of drug efficacy against Mycobacterium tuberculosis using an improved firefly luciferase. *J. Antimicrob. Chemother.* **2013**, *68*, 2118-2127.

34. Tiaden, A. N.; Kessler, A.; Hilbi, H. Analysis of legionella infection by flow cytometry. *Methods Mol. Biol.* **2013**, *954*, 233-249.

35. Tiaden, A.; Spirig, T.; Weber, S. S.; Bruggemann, H.; Bosshard, R.; Buchrieser, C.; Hilbi, H. The Legionella pneumophila response regulator LqsR promotes host cell interactions as an element of the virulence regulatory network controlled by RpoS and LetA. *Cell. Microbiol.* **2007**, *9*, 2903-2920.

36. Wiegand, I.; Hilpert, K.; Hancock, R. E. Agar and broth dilution methods to determine the minimal inhibitory concentration (MIC) of antimicrobial substances. *Nat. Protoc.* **2008**, *3*, 163-175.

37. Eloff, J. N., A sensitive and quick microplate method to determine the minimal inhibitory concentration of plant extracts for bacteria. *Planta Med.* **1998**, *64*, 711-713.

38. Kaminskyy, D.; Zimenkovsky, B.; Lesyk, R. Synthesis and in vitro anticancer activity of 2,4-azolidinedione-acetic acids derivatives. *Eur. J. Med. Chem.* **2009**, *44*, 3627-3636.

39. Humphrey, W.; Dalke, A.; Schulten, K. VMD: visual molecular dynamics. *J. Mol. Graph.* **1996**, *14*, 33-38, 27-28.

40. Wolber, G.; Langer, T. LigandScout: 3-D pharmacophores derived from protein-bound ligands and their use as virtual screening filters. *J. Chem. Inf. Model.* **2005**, *45*, 160-169.

Scheme 1

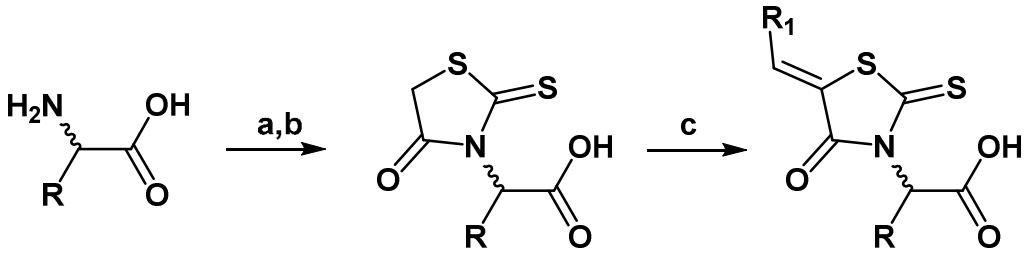

1 - R= $-CH_3$, R^1= $-C_6H_5N(CH_3)_2$; **2** – R= $-CH_2CH_3$, R^1= $-C_6H_5N(CH_3)_2$; **3** - R= $-CH(CH_3)_2$, R^1= $-C_6H_5N(CH_3)_2$; **4** -, R=$-CH_2CH(CH_3)_2$, R^1= $-C_6H_5N(CH_3)_2$; **5** - R= $-CH_2CH(CH_3)_2$, R^1= $-C_6H_5N(CH_3)_2$; **6** - R= $-CH(CH_3)CH_2CH_3$, R^1= $-C_6H_5N(CH_3)_2$; **7** – R= $-(CH_2)CH_3$, R^1= $-C_6H_5N(CH_3)_2$; **8** - R= $-(CH_2)_3CH_3$, R^1= $-C_6H_5N(CH_3)_2$; **9** – R= $-(CH_2)_2SCH_3$, R^1= $-C_6H_5N(CH_3)_2$; **10** – R= $-(CH_2)_2SeCH_3$, R^1= $-C_6H_5N(CH_3)_2$; **11** - R= $-CH_2COOH$, R^1= $-C_6H_5N(CH_3)_2$; **12** - R= -indonyl, R^1= $-C_6H_5N(CH_3)_2$; **13** - R= $-CH_2CH(CH_3)_2$, R^1= $-C_{10}H_6N(CH_3)_2$; **14** - R= $-CH_2CH(CH_3)_2$, R^1= $--C_{10}H_6N(CH_3)_2$; **15** - R= $-(CH_2)CH_3$, R^1= $-C_{10}H_6N(CH_3)_2$; **16** - R= $-(CH_2)_3CH_3$, R^1= $-C_{10}H_6N(CH_3)_2$; **17** - R= indonyl, R^1= $-C_{10}H_6N(CH_3)_2$; **21** - R= $-CH_2CH(CH_3)_2$, R^1= $-C_6H_5N(C_2H_5)_2$; **22** - R= $-CH_2CH(CH_3)_2$, R^1= $-C_6H_5SCH_3$; **23** - R= $-C_6H_5F$, R^1= $-C_6H_5SCH_3$; **24** - R= indonyl, R^1= $-C_6H_5N(C_2H_5)_2$; **25** - R= -indonyl, R^1= $-C_6H_5C_3H_7$; **26** - R= -indonyl, R^1= $-C_6H_5N(C_2H_4Cl)_2$; **27** - R= -indonyl, R^1= $-C_6H_5C_3H_7$; **28** - R= -indonyl, R^1= $-C_6H_5N(C_2H_4Cl)_2$; **29** - R= -indonyl, R^1= $-C_6H_5Cl$; **30** - R= -indonyl, R^1= $-C_6H_4Cl_2$; **32** - R= -indonyl, R^1= $-C_{14}H_8Cl$; **33** - R= -indonyl, R^1= $-C_{10}H_6CH_3$; **34** - R= -indonyl, R^1= $-C_{10}H_6CH_3$.

Reagents and conditions: a) CS_2, KOH, room temp. 4 h.; $ClCH_2COOK$ room temp., 30 min.; b) 6N HCl 90 °C 5-30 min.; c) Knoevenagel condensation: AcOH, AcONa, Aldehyde, 100 °C, overnight.[38]

Table 1. *In vitro* activity of the most potent InhA inhibitors **12**, **16-18**, **21**, **24-30**, **32-34**. IC_{50} values correspond to the concentration of the compound that inhibited *Mtb* InhA activity by 50%. The effect of all the compounds against *Mm* virulence has been tested at 10 μM concentration.

Compounds	***Mtb* InhA IC_{50} (μM)**	***Mm* MIC (μM)**	***Ef* MIC**	***Mm* anti-virulence visualization**	***Mm* anti-virulence evaluation**
12	28.6 ± 1.3	22.17	-[a]		0
16	24.4 ± 0.3	2.33	-		0
17	19.1 ± 1,3	1.99	-		4
18	19.1 ± 1.3	21.55	-		1
21	22.4 ± 1.5	2.46	-		4
24	14.7 ± 2.2	2.08	-		2
25	13.0 ± 2.1	22.22	-		3
26	12.2 ± 1.6	1.82	-		3
27	13.0 ± 2.1	55.55	-		3
28	15.2 ± 2.4	18.28	-		4
29	19.7 ± 1.4	21.05	-		4
30	9.5 ± 2.2	21	-		4
32	2.9 ± 0.7	184.5	0.312 μg/ml (0.57μM)		4
33	8.7 ± 0.5	0.21	1.25μg/ml (2.6μM)		4
34	11.0 ± 0.7	2.11	2.5μg/ml (5.2μM)		4
Triclosan	6.1 ± 2.1	8.63-	-	-	-
Amikacin	-	1.7	-	-	-

[a] "-" means not determined.

Table of Contents

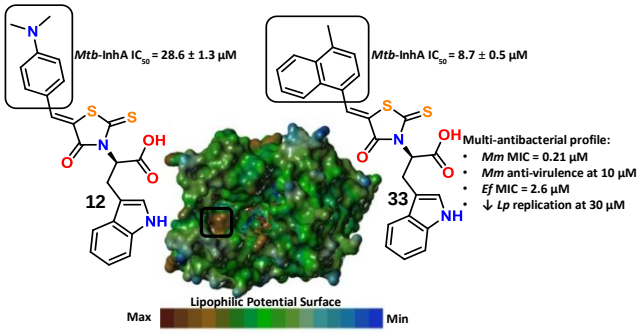

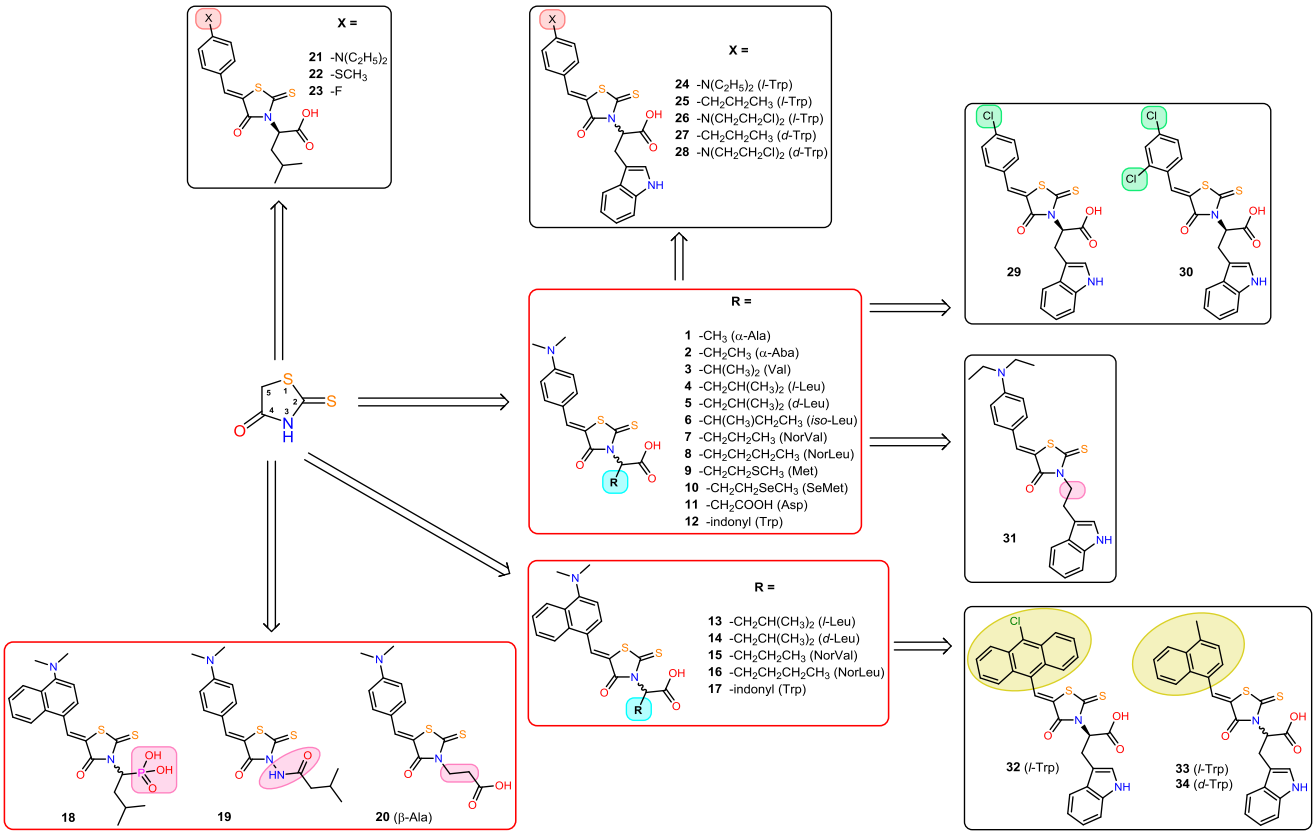

Chart 1. Design strategy for rhodanine-based ligands based on the first (derivatives **1-20**; red boxes) and the second (derivatives **21-34**; black boxes) series. The first series was synthetized by introducing different amino acids with various side chains at position *N*-3 (highlighted in blue; aliphatic chain: **1-11;** chain length: **1-10** and **19-20**; branched chain: **3**, **5-6**; aromatic ring: **12**) or by introducing more lipophilic naphthylidene ring at the position 5 (derivatives **15-18**, **20).** Modifications carried out on the carboxylic function are highlighted in magenta (**18-20**). The second series was optimized by maintaining the tryptophan residue at the position *N*-3 and modifying the substituent of the position 5 of rhodanine with arylidene ((highlighted in pink: **21-25**, **27**), polycyclic 10-chloro-anthracenylidene (**32**) and 4-methyl-naphthylidene (**33** and **34**) rings are highlighted in gold. The chlorinated substituents of derivatives **29** and **30** are highlighted in green. The loss of the carboxylic function in the compounds **31** is marked in violet.

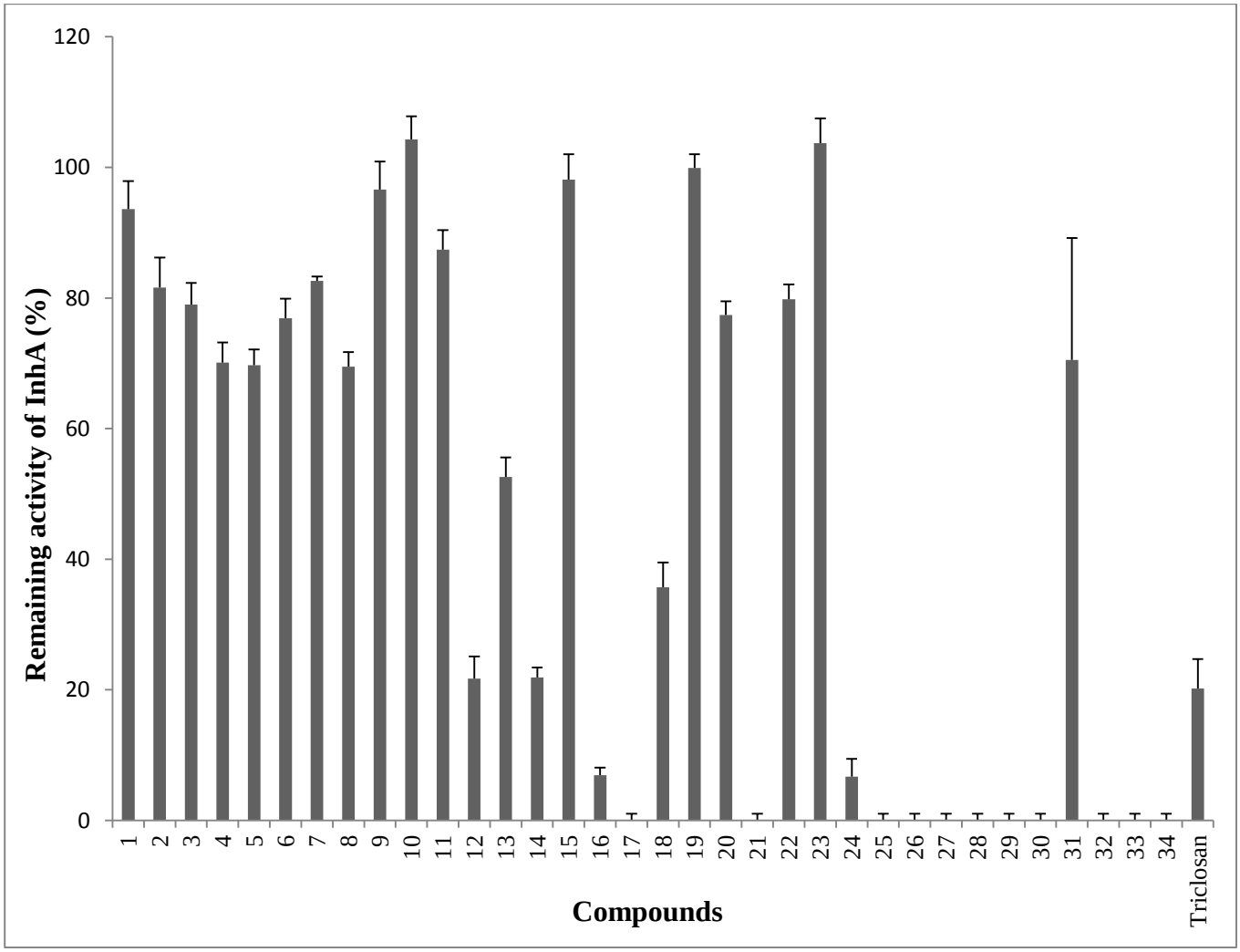

Figure 1. Inhibitory activity of synthetic derivatives (at 30 μM) towards InhA. InhA inhibition is presented as remaining activity. Several synthetic rhodanine derivatives possessed slight inhibitory activity at 30 μM. Compounds **17**, **21**, and **25-30 32-34** were the most active and totally inhibited InhA activity. Exact numbers are reported in Supporting Table S1.

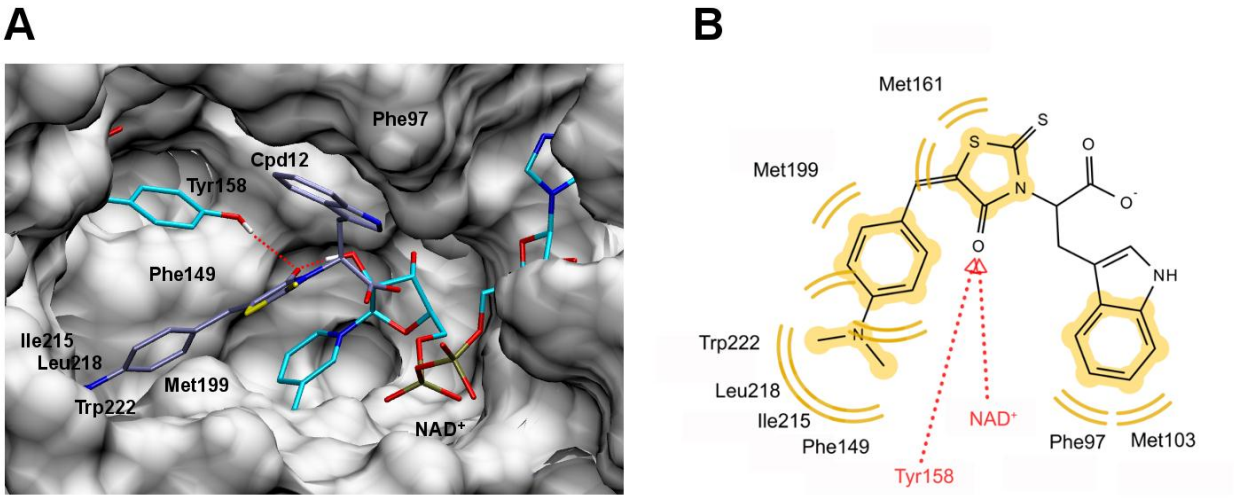

Figure 2. Panel A shows the binding mode of ligand **12** in the active pocket of InhA visulized by VMD.[39] Ligand **12** is color-coded by atom type (nitrogen in dark blue, oxygen in red, sulfur in yellow) with the carbon atoms in iceblue. Tyr158 and NAD^+ are colored by atom type with carbon atoms in cyan. Hydrogen bonding is displayed as red dots. Panel B shows a schematic representation of contacts between **12** and the binding site residues of InhA visualized by LigandScout.[40] The H-bond interactions between the inhibitor **12** and the residue Tyr158 and NAD+ are presented as red dotted arrows. The InhA binding site residues establishing hydrophobic and Van der Waals contacts with the compound **12** within a maximum distance of 4.0 Å are also displayed.

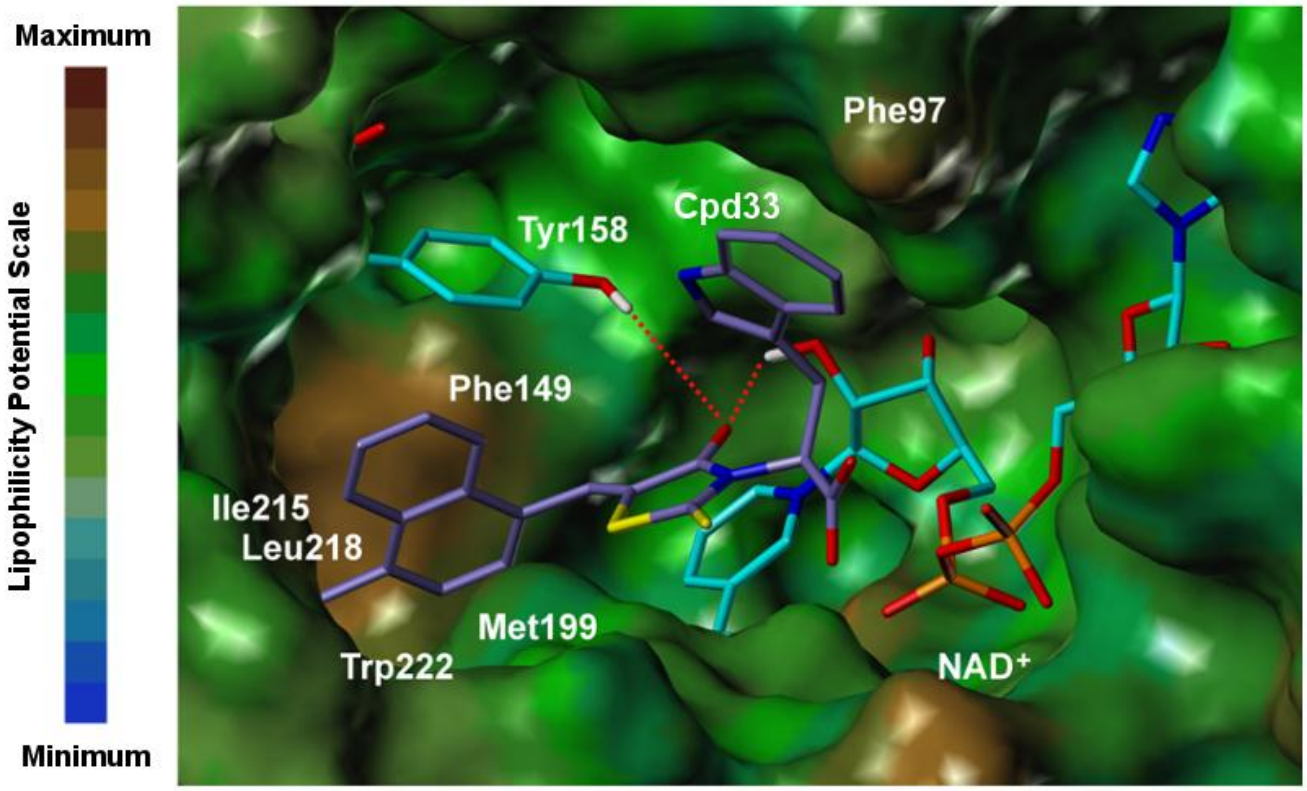

Figure 3. Lowest energy docking model of derivative **33** in the binding pocket of InhA represented as Lipophilic Potential surface calculated by the means of SYBYL 2.1.1.[31] On the left, the lipophilicity scale is presented (max = brown; min = blue). Ligand **33** is color-coded by atom type (nitrogen in blue, oxygen in red, sulfur in yellow) with the carbon atoms in iceblue. Tyr158 and NAD^+ are colored by atom type with carbon atoms in light cyan. Hydrogen bonding interactions are displayed as red dots. The hydrophobic interactions of **33** with side chains of Phe149, Met199, Ile215 and Leu218 are highlighted.

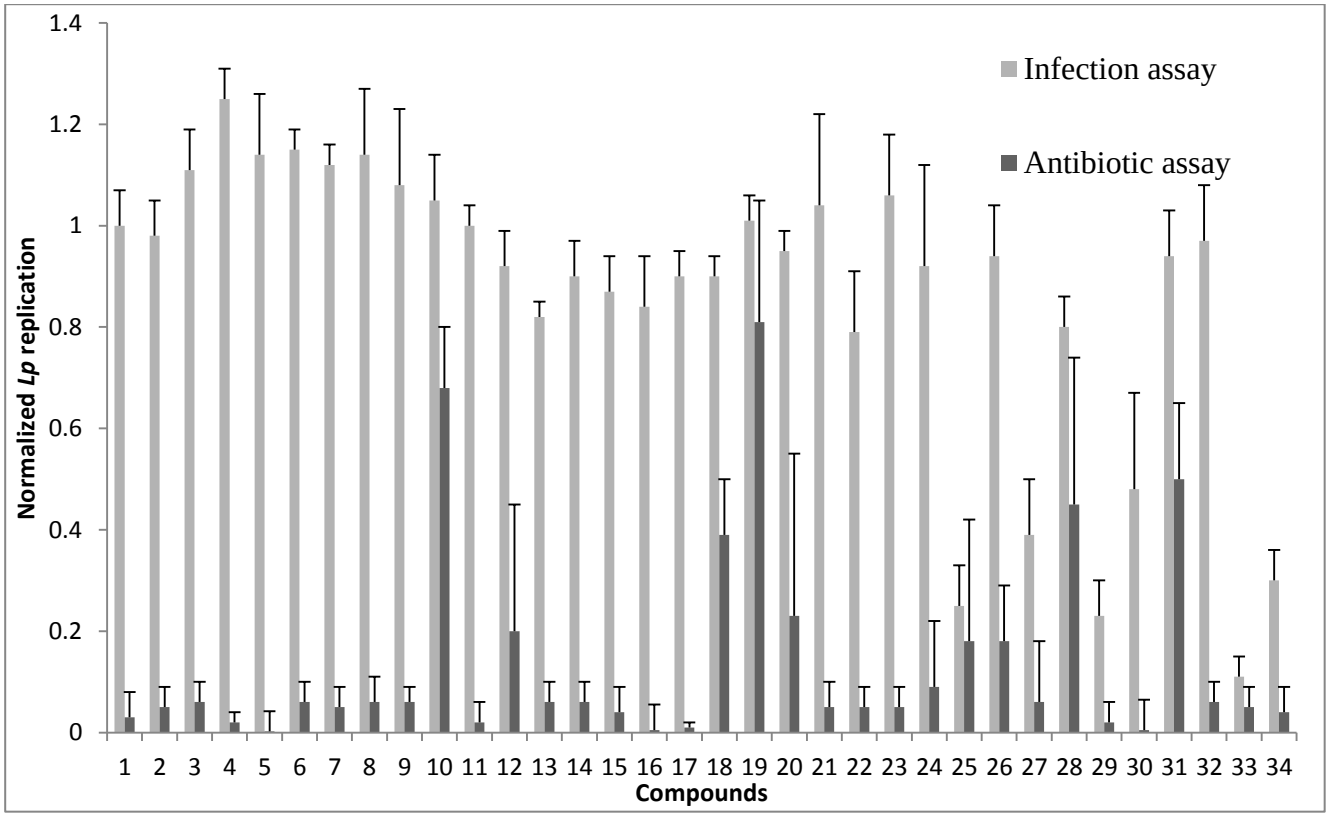

Figure 4. Antibiotic and anti-infection activities of compounds **1-34** (at 30 μM) represented as inhibition of *Lp* replication. The values are presented as extracellular (Antibiotic Assay) and intracellular (Infection Assay: the *Acanthamoeba castellanii* amoebae represents the host cell) normalized *Lp* replication.[27] All graphs indicate the combined averages of at least 3 independent experiments. Exact numbers are reported in the Supporting Table S2.